POLITECNICO
MILANO 1863

ON THE PROPERTIES OF NEW SUSTAINABLE CEMENTITIOUS COMPOSITES

MSc Thesis by Teresa Karoline Forstner (943260)

November 2021

ADVISOR

Prof. Valter Carvelli

CO-ADVISOR

Prof. Claudia Marano

Hoang Nguyen (University of Oulu, Finland)

POLITECNICO DI MILANO

BUILDING ENGINEERING

Table of Contents

Tables

Figures

Abstract

Cement and cement products such as mortar and concrete are a major global contributor to greenhouse gas emissions. However, they are indispensable as construction materials especially in developing countries. To reduce the environmental impact of the cement industry, a significant research effort is currently put into the development of a more sustainable alternative to conventional mortar and concrete, which is at the same time affordable and accessible. This paper investigates the use of carbonated and recycled steel slags as a replacement for clinker and aggregate in mortar or concrete.

Three types of slags, Blast Oxygen Furnace Slag (BOF), De-Sulfurisation Slag (De-S) and Ladle Slag (LS) were sourced in Finland and sent to Politechnico di Milano for mixing and testing, after they were pre-processed and carbonated at the University of Oulu. Several different composite materials were sampled from the available slags, and were tested for compressive strength, stress-strain behaviour, thermal degradation, and frost resistance.

After the initial experiments with LS-based composites proved unsuccessful, the research was continued using conventional cement clinker with De-S slag as aggregate. The performance of the cement-based samples showed more promising results – while relatively weak in compression and of low stiffness, the material performed very well in freeze-thaw tests, showing no loss of strength or degradation of the material after 28 cycles.

Overall, the material may be suited for non-structural applications, such as low-grade concrete or mortar. Further research is needed to identify possible changes to the material composition that could improve the properties especially regarding compressive strength and stiffness.

1. Introduction

Currently, much of the world's construction effort relies on concrete and other cementitious products. In fact, concrete is the most consumed material globally, second only to water. Unfortunately, the emissions associated with the production of cement are major – to reach environmental goals and contribute to efforts of reducing climate change, these emissions need to be mitigated. Therefore, many possible alternatives to conventional cementitious construction materials were investigated in recent years, using recycled and carbonated materials to substitute cement or concrete aggregates.

This thesis aims to contribute to such efforts by investigating new cementitious materials. For this, three types of steel slag are sourced from steel manufacturing plants and pre-processed at the University of Oulu in Finland and sent to the Politecnico di Milano for mixing and testing. The research focuses on the performance of different material configurations using the various types of slags, and an assessment of their environmental impact and suitability as an alternative to concrete or mortar.

Firstly, current and past research on the topic is summarised in a literature review. This includes different approaches to the problem and an overview of materials currently used and developed for this application. Then, the project is introduced, and the experiments outlined. In the main body of the paper, the experimental procedure and the results are stated. This is comprised of a detailed description of the materials and preparation process, followed by results for compression testing, durability and TGA analysis. The environmental impact of each material configuration is estimated and compared to a conventional mortar mix. Finally, the conclusions are summarised, and suggestions are given for future research.

Literature Review

2. Environmental Impact of the Cement Industry

Concrete is the most widely used construction material in the world, due to its availability, low cost, easy handling and applicability. In 2019, it was estimated that 4.1 Gt of cement were produced, with this number expected to rise moderately in the next decade, especially in developing countries such as India and many African countries (Levi, et al., June 2020), and some sources claiming an increase of up to 4.68 Gt/year by 2050 (OECD/IEA, CSI, 2018). Unsurprisingly, the cement and concrete industry is also the 3rd largest industrial energy consumer and major contributor to CO2 emissions, making up 6–7% of global anthropogenic CO2 emissions (OECD/IEA, CSI, 2018), with some papers even citing a higher contribution, depending on how the CO2 emissions are allocated during the process. However, ordinary Portland cement (OPC) will remain essential for low-cost buildings and infrastructure systems, and hence is irreplaceable especially for the growth of developing nations. Efforts to reduce the environmental impact of the cement industry are with regards to the Paris Agreement, limiting the global temperature increase by 2°C by 2100 and more importantly, the EU's 2030 energy framework to reduce greenhouse emissions by 40% from 1990 levels (European Commission, 2021).

To meet this goal, a large research effort has been made to identify possible solutions and mitigation methods, that reduce the impact of the industry while maintaining the availability and low cost of concrete as a construction material.

2.1 CO_2 generation in cement production

Cement hydrates are formed from the hydration between water and cement. Ground cement is manufactured from clinker and various admixtures such as gypsum and fillers (slag, fly ash). Portland cement is a Ca-based binder that needs Ca to form various calcium silicates during the clinkering process in rotary kiln. Calcium carbonate is the main source of Ca in Portland cement clinker, in which the calcination of $CaCO_3$ releases CO_2 starting at 800 °C.

The emissions associated directly with cement clinker production are due to two factors: (I) the combustion and oxidation of fuel during manufacture and (II) the chemical and physical processes of converting the raw materials into cement clinker. The CO_2 emissions generated in the production of OPC clinker are estimated at 842 kg CO_2/t by the Cement Sustainability Initiative ((CSI), 2016). Indirect CO_2 emissions are related to deforestation, production of electrical energy, and transport. Often powered by fossil fuels, cement clinker production requires high temperatures and consequently a significant amount of fuel. However, this still only amounts to about a third of CO_2 released in the production. The remaining fraction of

emissions are due to the reaction in the material, namely the decomposition of calcium carbonate into calcium oxide and CO_2 in the calcination process:

$$CaCO_3 + heat \rightarrow CaO + CO_2$$

The resulting lime (CaO) reacts with the silica, aluminium and materials containing iron in a mineralisation process to produce clinker. Ordinary Portland cement (OPC), the most widely used and standardised type of concrete, contains around 95% of clinker and 5% gypsum, but can also be blended with other types of materials.

3. Measures to reduce CO_2 intensity in concrete production

Several strategies are currently in place to reduce CO_2 emissions produced by the concrete industry. They can be roughly separated into direct approaches that aim to reduce the direct emissions, and indirect approaches, aimed at reducing indirect emissions, improving the materials life cycle, such as elongating service life and recycling, and innovative carbon sequestration and reuse technologies.

3.1 Indirect CO_2 reduction measures

While all efforts remain important in reducing the environmental impact of cement, the aforementioned indirect methods are beyond the scope of this paper.

However, one indirect method worth noting is the re-carbonation of concrete structures and products over their life cycle. This is a reaction of CO_2 with the concrete that occurs naturally over many years, as it penetrates the concrete surface and reacts with the hydration products, forming mainly calcium carbonate. This is associated with degradation of the concrete as it can cause corrosion of reinforcement steel below the surface, however for unreinforced concrete, carbonation is no cause for concern and may even improve the mechanical properties. (Andersson, et al., 2019)

As CO_2 penetrates the concrete, it reacts with the hydration products. The principal reaction is with $Ca(OH)_2$ and the secondary with C-S-H gel.

[1] $Ca(OH)_2 + CO_2 \rightarrow CaCO_3 + H_2O$ (1)

[2] C-S-H + + $CO_2 \rightarrow CaCO_3$ + amorphous SiO_2 +H_2O

The carbonation reaction however is not currently used in the calculation of the net CO_2 emissions of concrete. This is despite the fact that CO_2 captured in concrete will remain there unless it is heated to calcination temperature, and higher carbonation rates can be achieved in crushed concrete at the end of its life cycle due to the higher surface area. (Andersson, et al., 2019) In fact, concrete at its end-of-life stage has high potential to be used as a carbon sink, not only due to the naturally occurring carbonation of crushed and disposed concrete, but also through enforced carbonation and carbon capture and reuse as a clinker replacement. (Zajac, et al., 2020) This can be done for several other materials and will be discussed further later on.

3.2 Direct CO_2 reduction measures

Successful efforts regarding the reduction of CO_2 in the manufacturing phase have been regarding the increase of energy-efficiency and replacement of fossil fuels, where improvements have already reduced the CO_2 emissions by 50% since the 1960s. *"Reducing the share of fossil fuels in the cement industry globally to 24% by 2050 would reduce the CO_2 intensity of the global thermal energy demand from 0.088 t CO_2/ GJ to 0.058 t CO_2/GJ"* – (Andersson, et al., 2019). The highest CO_2 production comes from wet-kilns, that have been

effectively eradicated in Europe, while high-efficiency kilns have been adopted widely even in developing countries. Further steps such as the use of alternative fuels (eg biomass), electrification and waste heat recovery are underway, but in general, much has already been done in this regard and further innovation in the area of energy efficient kiln/heating are stagnating and breakthrough technologies are currently not on the horizon. (Cembureau, 2018)

Of course, even the best efforts of reducing fuel-related emissions will not be enough, as this aspect only accounts for about one third of emissions in cement production. Ultimately, the highest reduction potential lies in raw material efficiency, namely (I) replacing raw materials in cement clinker, and (II) blending OPC clinker with suitable supplementary cementitious materials (SCM), reducing the overall clinker-to-cement ratio. The latter is by far the most efficient measure to reduce CO_2 emissions, since it reduces both the CO_2 from the raw materials as well as from fuel combustion. Considering fly ash as an SCM, a replacement fraction of 25-25 wt.% can save up to 90kg CO_2/t of direct emissions in cement production compared to pure OPC. Challenges to this approach are the availability of alternative materials, performance and durability requirements and consequently the standards and market acceptance of the product. (Schneider, 2019)

(I) Alternative cementitious binders

With the most prominent binder being OPC clinker, which is predominantly limestone, there are several alternatives summarised by (Scrivener, et al., 2018) and (Andersson, et al., 2019), that exhibit a similar composition and properties to cement clinker:

Belite clinker: contains 40-90% belite and trace of alite.

The advantage of this clinker is that it can be produced in a conventional kiln at a lower lime saturation setting, which reduces the emissions caused by the fuel, resulting in CO_2 savings reduction of up to 10% compared to OPC. However, the clinker's lower grindability can cause additional emissions due to increased need for electrical energy and they exhibit very slow strength gain.

Calcium sulphoaluminate (CSA) clinker/cements: contain as main phases ye'elimite, belite and gypsum. CSA clinkers are a more effective alternative to Belite clinkers, being less CO_2 intensive and also setting and developing strength quicker. However, the addition of Bauxite leads to far higher production costs.

Furthermore, Alkali-activated binders (geopolymers), produced by activating a reactive alumina-silicate using an alkaline component, have some potential to contribute to the CO_2 reduction of the concrete industry, however at present require similar raw materials as also used in blended cements to reduce the clinker to cement ratio, such as natural pozzolans or GGBFS, and diverting those materials may have an overall bad impact.

(II) Reducing Clinker-To-Cement Ratio

The measure of the most impact, and first key action of the technology roadmap for 2030 (OECD/IEA, CSI, 2018), is the reduction of the clinker fraction in Portland cement from the global average of 0.65 in 2014 to 0.64 in 2030, producing blended Portland cement with comparable properties. Conventional OPC is made of clinker and 4-5% of gypsum, but other materials can be added in to reduce the fraction of clinker and produce blended cement of similar properties and durability. In fact, it is developing countries such as China and India that produce concrete with lower clinker-to-cement ratios, while the European average is around 0.78 in 2018, with some countries such as Ireland and Denmark producing with a ratio of 0.9 (all data: https://gccassociation.org/gnr/; (Schneider, 2019)). The limiting factor for reducing this ratio is not the cost, but the availability of suitable materials that maintain the desired quality of the concrete.

The materials used for this application are referred to as supplementary cementitious material (SCM) and as such exhibit either pozzolanic or hydraulic activity. Pozzolans are materials high in silica and alumina that react in the presence of water with dissolved calcium hydroxide to form compounds of cementitious properties, so-called C-A-S-H phases. Hydraulic SCMs react with water to form a calcium-silicate-hydrate (C-S-H) gel which acts as a cementitious material. (Thomas, 2007), (Schneider, 2019)

The main materials that have been researched for this purpose are steel/iron slags (several types), fly ash, pozzolans, calcined clays and blends.

Blast Furnace Slag

Blast furnace slags are a by-product of the reduction of iron, with the main subcategories being ABS (air cooled blast furnace slag) and GGBFS (Ground granulated blast furnace slag). BF slags show very good properties and durability, as additions to clinker as well as blended cement at high ratios of up to 70%. (Scrivener, et al., 2018) However, it would be a mistake to label BF slags as a waste material, as GGBFS requires immediate processing and is sold by iron manufacturers. However, there is little potential for increasing CO_2 emissions further with this, as >90% of available blast furnace slag is already being used as addition to cement or concrete. (Scrivener, et al., 2018)

Fly Ash

Fly ash is a by-product, obtained by the precipitation of unburned coal particles from the flue gases in furnaces. Depending on the coal type used in combustion, it can be either classified as siliceous or calcareous, with the former containing predominantly silica and alumina, and the latter free lime oxide, resulting in pozzolanic or hydraulic reactivity respectively. Siliceous fly ashes in particular are used widely as SCM and can replace clinker in cement with roughly 15-50 wt.%, with higher levels (>30%) used in structures to control temperature rise and even 60% proved to show good mechanical properties in structural applications. In general, fly ash

in cement improve the workability, long-term strength and durability of concrete, however higher ratios tend to result in slow strength development and setting times, as well as reduced durability (Thomas, 2007). According to research by (Schneider, 2019), considering a reference clinker factor of 0.75, “the increase of the share of fly ash in cement of up to 25–35% would lead to a decrease in direct CO_2 emissions from cement production of up to 90 kg CO_2/t cement”. Fly ash is also widely available; however, this may become less as coal-firing plants are coming out of use.

Natural Pozzolans/Thermally Treated Clays

Natural pozzolans can be of volcanic origin and sedimentary rocks, as well as thermally treated calcined clays or shales. Like fly ash, moderate amounts of the material yield improvements over standard Portland cement in durability and strength development, as well as chemical resistance. A limiting factor however is the tedious production and pre-treatment, as well as regional availability in case of volcanic rock. (CSI/ECRA, 2017)

Silica Fumes

Silica Fumes are a by-product from Silicon-containing metals manufacture. It was previously released into the atmosphere, however it is now being captured and re-used in the production of cement. Using the right ratio, silica fume can improve many characteristics of the concrete, such as reducing permeability, increasing strength and workability. However, the availability is limited and depending on the local industry. In its current capacity, it is already an established and widely used additive. (Mann, 2014)

Recycled Concrete Fines

As mentioned previously, recycling and reusing concrete as aggregate or SCM has tremendous potential to reduce CO_2 emissions. It is readily available at a global scale and additionally has the ability to capture carbon. This happens naturally at a slow pace but can be enforced during production. Experiments show that the crushing, grinding and hydrating produces a cement paste that can spontaneously bind CO_2 by forming calcite and other carbonation products, depending on the composition and carbonation environment. (Zajac, et al., 2020)

Many more sources of SCMs are constantly being proposed and tested, for example pumice, perlite and vitric ash, that show high pozzolanic activity and similar performance to fly ash. Those are natural SCMs which could potentially be sourced from industrial waste/overburden, but in most cases have to be quarried, transported and processed which makes this a very costly alternative.

Other potential SCMs from waste products include agricultural waste ashes, biomass fuel ashes, municipal waste sludge ashes, oil shale waste and waste glass.

Finally, fillers such as clay and limestone can be used to replace clinker, with substitution rates of up to 50% while maintaining strength levels comparable with that of OPC. (Schneider, 2019)

In fact, a limestone/calcined clay blended cement LC^3 has been developed, which replaces OPC clinker by 50% while achieving the same properties as a 30% fly ash replacement and reducing CO_2 emissions by up to 40%. This material has been applied successfully in several trials and is on its way to be accepted by the standards. (Juenger, et al., 2019)

(III) Steel Slag Clinker Replacement and Carbonation

This is by far the most interesting group of SCM's, since they not only aid in reducing the clinker-to-cement ratio, but also are suitable for carbonation, which is a reaction that can be induced in some materials to capture CO_2 and in the process improve the properties of our concrete, thanks to steel slags composition, mineralogy and availability. Steel slag is a hydraulic material, as it contains dicalcium (C_2S) and tricalcium (C_3S) silicates that can react with water to form C-S-H gel, which can be used as a cementitious material. However, steel slag exhibits rather slow hydration and potential expansion/volume instability, due to high amounts of free lime and magnesium oxide. Fortunately, this can be solved by carbonation, due to the carbonation reaction being much faster than the hydration reaction, and the carbonation of free oxide will improve volume stability. According to previous studies and as will be discussed in subsequent chapters, the C-S-H gel silicates formed in the hydration of steel slag react with CO_2 to form carbonates such as $CaCO_3$ (Wang, et al., 2019). Research on steel slag binders such as by (Wang, et al., 2019), shows that CO_2 uptake can improve compressive strength as well as shrinkage and freeze-thaw resistance.

Slags are a by-product of steel manufacture and are typically classified by the type of furnace. Unlike blast furnace slags, that are already commercialised, steel slags are still being investigated as potential SCMs.

Electric Arc Furnace

EAFS-S and EAFS-C are types of steel slag produced by melting steel scraps using electric arcs and combining this with other additives like lime and dolomite. EAF slags are widely available where electric arc furnaces are used for steel production and rarely recycled especially in developing countries, but as with many steel slags, the main obstacle to widespread use is the variability in chemical composition and consequently properties. They are currently predominantly used directly in low-value applications such as mortars, aggregates and as filters in water treatment, as higher-value applications require further processing and quality control. (Teo, et al., 2020)

(IV) Steel Slag Clinker/Aggregate Replacements used in this project

Three types of steel slags were used in the scope of this project, namely BOF slag, ladle slag and De-S slag. The latter has not been researched to the same degree as BOF and ladle slags and is thus of high research interest.

Basic Oxygen Furnace

BOF slag is the result of the conversion of pig-iron to steel by blowing oxygen, and hence contains a rather high amount of iron, as well as free lime, portlandite, Ca- silicate (C_2S) and Ca-ferrite (C_2F). It is widely available, accounting for 74% of all types of steel slags globally. (Wang, et al., 2019) This type of steel slag is especially suitable for carbonation due to its high alkalinity and high Ca-content (Huijgen, et al., 2005), reaching up to 20wt.% of carbonate content. Furthermore, according to a study by (Librandi, et al., 2019), the CO_2 uptake is positively correlated with a 39-fold increase in compressive strength, which however still remained lower than that of the carbonated EAF slag.

Ladle Furnace

Ladle furnace slag is a steel slag containing over 50% of CaO as well as silica and alumina. Unlike BOF and EAF, ladle slag is basic and contains less iron, but higher content of free lime and calcium. It is widely and cheaply available from steel manufacturing, with up to 30 kg of ladle slag produced from every ton of steel, and mostly disposed as waste in landfills. (Mahoutian, et al., 2014) (Nguyen, et al., 2019). However, the properties of the slag are very variable and depend on the chemical composition of the individual sample and has been predominantly applied in mortar and other low-value applications. Depending on properties however, LS with high silica content can be blended with GGBFS and alkali-activated for use as a binder, as well as carbonated to increase strength (Mahoutian, et al., 2014). Other studies by (Nguyen, et al., 2019) (Nguyen, et al., 2019) also show promising research on alumina-rich ladle slag with gypsum (LSG) which acts as a hydration catalyst, and citric acid to yield a high-performance ettringite-based binder that shows comparable properties to OPC with a much decreased CO_2 intensity.

De-Sulfurization

A relatively unknown steel-manufacture by-product is De-sulfurization slag (De-S). It is a result of hot metal pre-treatment, where the liquid steel is deoxidised and stirred with a lime-rich slag to remove Sulphur (Bogala, et al., 2015). Despite the high iron content of the De-S slag, it is rarely recycled for steel manufacture due to the high sulphur content. In rare cases, it is used in wastewater treatment and in small amounts, as raw material in concrete, but due to the lack of research and recognition it usually goes to waste (Chen, et al., 2018). Overall, De-S has very similar chemical composition to EAF and BOF slags, with high CaO, Fe_2O_3 and SiO_2 content.

4. Project Aims and Objectives

4.1 Overview

This thesis project is focusing on measurements of some properties of a new cementitious composite manufactured at the 'Fibre and Particle Engineering Research Unit' of the University of Oulu, Finland, from Basic Oxygen Furnace Slag, or De-Sulfurisation Slag, using a ladle slag binder. The materials are hydrated and carbonated at the University in Finland, following which the samples are transferred to Politecnico di Milano, where they will undergo microscopic, mechanical and durability tests in order identify the relevant properties for possible uses for building application. The aim is to use the final material as aggregate for brick and contribute to efforts of finding feasible low-carbon alternatives to commercial Portland cement products.

4.2 Material

The main material to be researched is the basic oxygen furnace/de-sulfurisation steel slag such as the ones identified previously, which results from the conversion of pig-iron to steel in the steel manufacturing process. It can be sourced from a local steel manufacturing plant and processed to create a cementitious composite, which could potentially be applied as a low-CO_2 intensive alternative material in mortars or even as clinker addition or replacement in concrete.

(V) Expected Composition and Control Parameters

While the exact composition is identified in Table 3, BOF and De-S slags are typically an alkaline material, composed mainly of CaO, Fe_2O_3 and SiO_2.

As described by (Wang, et al., 2019), BOF as well as De-S slags initially do not have the qualities desired in a SCM, as they exhibit poor compressive strength, volume instability due to free CaO and MgO, are highly alkaline and as a result are prone to leaching of trace metal ions, that could cause environmental damage. However, it has been shown that accelerated carbonation of BOFS could solve these issues as well as act as a carbon capture mechanism. As previously discussed, BOFS is suitable for carbonation, more so than other steel slags, due to the high reactivity of metal oxides such as CaO and MgO and their hydrates (in particular *portlandite* $Ca(OH)_2$) with CO_2. During this process, those metal oxides which were previously responsible for the volume instability of BOFS, are transformed into thermodynamically and chemically stable carbonates (Librandi, et al., 2019). The carbonation process can be described

with the following reaction of Ca and/or Mg ions from alkaline silicate minerals with CO_2, producing carbonates such as $CaCO_3$ (Quaghebeur, et al., 2015):

$$(Ca, Mg)_x Si_y O_{(x+2y)} + xCO_2 + H_2O \rightarrow x(Ca, Mg)_x CO_3 + ySiO_2 + H_2O$$

Carbonation also causes an increase of density in the material, increasing compressive strength considerably, to up to around 31 MPa according to studies by (Wang, et al., 2019) and (Librandi, et al., 2019), with subsequent hydration being able to further improve the strength to 36 MPa. The alkalinity is also reduced as a result of the consumption of the alkaline minerals in the carbonation reaction, which in turn reduces the leaching of metal ions. Furthermore, the formation of $CaCO_3$ coating also inhibits the leaching of alkaline minerals.

As all these reactions depend on the amount and availability of reactive chemical compounds, it can be deducted that the composition plays an important role in the material performance and reactivity.

4.3 Sample preparation and processing

The preparation and processing of the samples may be conducted similarly to the procedures outlined in research by (Quaghebeur, et al., 2015), (Wang, et al., 2019), (Librandi, et al., 2019) and (Huijgen, et al., 2005).

Preparation

Even though ladle slag tends to have a small particle size, it may be necessary to grind the material to the required size after the slag is dried. Then, some other ingredients may be added, and the particle size, mineralogy and chemical composition of the yielded homogeneous powder is subsequently analysed.

Carbonation and Hydration

After compacting the samples, they are carbonated at ambient pressure and temperatures of 40-60°C for 24-48 hours in 10-20% CO_2. After this, the carbonisation degree of the samples can be calculated based on their final composition. Then, hydration curing can be conducted to improve the properties of the material further. During this procedure, the samples are stored in air-tight containers for 0-360 days. However, in this project such long curing times are undesirable (Wang, et al., 2019).

4.4 Analysis & Testing Methods

Different tests can be run on the final product samples, depending on their composition and the available equipment at the lab. It is likely that the product will be more suitable for non-structural applications, and a comparison of the performance could be conducted with mortar or low-strength concrete. The following tests have been considered for analysis:

(VI) Compression tests

To determine material strength and to achieve an initial classification of the material as an alternative to conventional concrete and/or mortar, compression tests are conducted on samples of different curing time. The results expected from this analysis are maximum compression strength, stress-strain behaviour, elastic modulus and failure mode.

(VII) Material Degradation

To determine sample composition and assess the thermal stability and degradation of our material, a thermo-gravimetric analysis can be conducted. This analysis is done by measuring the weight of each component in a material as it volatilizes or decomposes under controlled conditions of temperature, time, and atmosphere. (TA Instruments, 2011)

(VIII) Durability Tests

For this application, an initial analysis of the freeze-thaw resistance of the material would be beneficial.

Freeze-thaw resistance

Due to the volumetric changes of water in the pores of hardened concrete in the freeze-thaw process, tensile stresses can occur, causing microcracks in the concrete structure. Scaling can occur on the surface of the concrete due to exposure to freezing temperatures, due to pressures generated by ice formation. This effect is heightened in the presence of de-icing salts, as salts reduce the meting point of ice, drawing the necessary heat for this from the material. Hence, a temperature gradient will form on the surface of the concrete, causing differential strains and stresses (Research, Development and Technology Turner-Fairbank Highway Research Center, 2002).

Freezing and cooling can be done with the specimen in tap water solution to simulate humidity or tap water solution with 3% of NaCl to simulate the presence of de-icing salts. Since we used demoulding agents on our samples, this can affect the scaling resistance and should be considered.

Furthermore, the scaling resistance test can be conducted according to (Setzer, et al., 1996) with the following expression:

$$m_c = \left(\sum \mu_s / A\right) \times 10^6 g/m^2$$

m_c = total amount of scaled material related to the test surface after c cycles in [g],
μ_s = mass of scaled material of the measurement after c cycles in [g] with an accuracy of 0.01 g. The sum is taken over all measurements until the nth cycle,
A = area of the test surface.

The measurements should be taken after 14 and 28 cycles, with the possibility of additional measurements after 4 or 6 cycles. It is calculated based on the linear dimensions, taken as the

average of at least two measurements determined to the nearest 0.5 mm. The mean value and the standard deviation of the scaled material should be evaluated. The mean value and the individual values for each specimen after 28 cycles are used for evaluating the scaling resistance.

In EN 13877-2, limiting values for acceptable and unacceptable scaling potential is specified for concrete pavements and the like, with good frost resistance resulting in < 0.10 kg/m^2 after 28 cycles for category FT1 and after 56 cycles for category FT2. It further specifies limits on the rate of scaling resistance loss.

Wet-Dry cycles

Cycles of wetting and drying can affect concrete by decreasing its durability and strength due to possibility of shrinkage-induced cracking. Concrete durability depends mostly on its resistance to water penetration. After the pores fill with water and the samples are subsequently dried, only the superficial area dries fully which leads to shrinkage in that part, while the internal part retains humidity and keeps the volume change. This leads to the formation of microcracks in the concrete. To test for degradation through this mechanism, samples are kept submerged in wetting solution and left to dry for some amount of time for several cycles, depending on the application of the concrete. Following the WD cycles, durability and strength can be tested by a compression test and measurement of weight.

The resistance of the samples can be evaluated by measuring the compressive strength, elastic modulus and evaluating mass loss after a number of aging cycles. The mass loss and density are evaluated by measuring the dimensions and weighting the samples before and after the WT degradation cycles and evaluating the average of percentage differences.

4.5 LCA

Upon completion of the experiment and testing, the net CO_2 is estimated as the difference of CO_2 produced during sourcing and processing of the material, and the CO_2 absorbed and stored during carbonation in the production stage. This way, a simple life cycle analysis focussing on equivalent embodied CO_2 is be prepared for the final product to determine the environmental benefit over conventional mortar.

5. Materials

The materials used throughout the process:

- Ladle Slag
- Basic Oxygen Furnace Slag
- De-Sulfurisation slag
- Portland Cement CEM I of 42.5 MPa and 52.5 MPa strength
- Gypsum, Citric acid, water

The ladle slag, BOF slag and De-S slag were delivered from the University of Oulu in Finland. The remaining materials were purchased in Milan.

6. Methodology

Preparation and testing of specimens were conducted approximately according to relevant standards on concrete testing (EN 1881) where applicable and based on recommended procedures outlined in previous research. Analysis and testing were conducted within the limits of available equipment such as moulds, tools, and machinery.

6.1 Particle size determination

The particle size distribution was conducted to determine the particle size ranges and gradation coefficient of our material. Particle size and grading affects the material in terms of density and air content and has a significant impact on the material strength. According to research by (Bentz, et al., 1999), smaller particle size is positively correlated with faster hydration and better early strength gain of material.

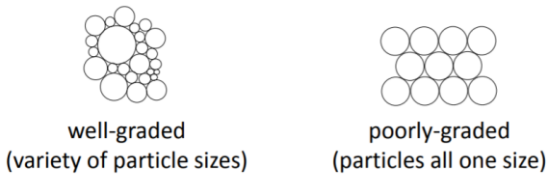

Figure 1: grading (Richardson, 2016)

The gradation coefficient indicates the range of particle sizes in a given sample and is calculated with the following formula:

$$Uniformity\ coefficient\ C_U = \frac{D_{60}}{D_{10}}$$

Where:

D_{60} = particle size [µm] passing at 60% cumulative weight
D_{10} = particle size [µm] passing at 10% cumulative weight

Different materials exhibit different types of gradation, including the following typologies:

- Dense or well-graded: $C_U > 4$
  Depending on the type of material, $C_U > 4$ indicates well graded gravel; $C_U >= 6$ well graded sand, while $C_U > 15$ non-uniform. This indicates a wide range of particle sizes, indicating less voids within the material. This could be useful when it comes to freeze-thaw and wetting-drying resistance of a material which will be discussed later in the paper.
- Uniform or poorly graded: $C_U =< 4$ or $=1$
  This is a type of gradation for materials of uniform grain size which does not apply in this case.

Material can also be gap-graded or open-graded; meaning missing a large chunk of particle sizes or particle distribution for high permeability respectively.

Coarse-grained or fine-grained materials depend on particle sizes, where fine-grained powders contain more than 50% of particles below the diameter of 75µm, while coarse-grained aggregates contain less than 50%.

(I) Ladle Slag

In preparation of the experiments, the ladle slag was first manually passed through sieves to determine particle size distribution. The material contained steel residue in larger aggregates which was removed using the 2mm sieve and discarded before the particle size measurement. The analysis was performed several times using 600-1000g batches of ladle slag for each measurement.

For particle size measurement, the following 5 sizes of sieves were used:

500µm – 250µm – 125µm – 106µm – 63µm

The sieving was conducted manually. Step by step, the material was passed through each sieve using shaking motion, starting with the largest sieve size to the smallest. Depending on the amount of material passing through the sieves, each sieve was shaken for 15-40 minutes at a time, as well as cleaned and unclogged periodically to ensure the maximum number of particles passing and a precise result. The remaining material in each sieve was weighted.

The particle size measurement results were collected in an excel sheet with cumulative results for each of the batches tested. The table with the recorded values can be found in the Annex.

Figure 2 shows the distribution of each measurement batch, with the dashed line indicating the average distribution. The results show some minor variations, that are potentially due to variable manual sieving times or slight variations in the composition of the batches. Overall, the results suggest relative homogeneity in particle size distribution.

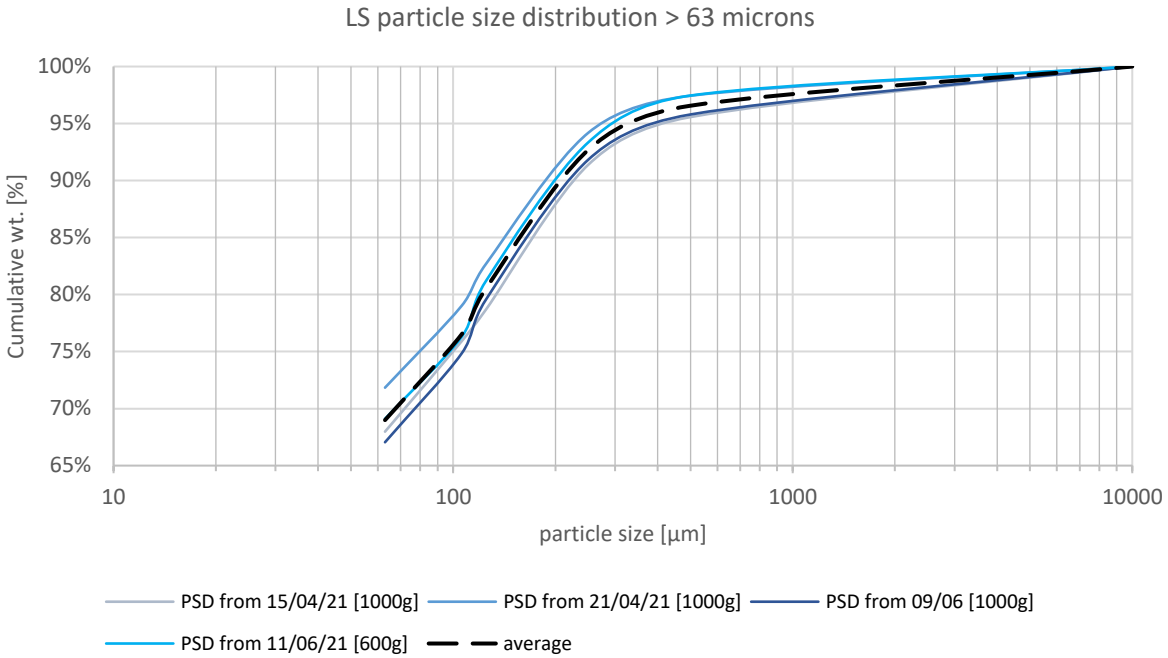

Figure 2: LS particle size distribution >63 microns

It is evident that between 69.1 and 72 wt% of the ladle slag is unaccounted for in the manual sieving process. This is due to the limitations of manual sieving for particle size analysis but will be accounted for using laser diffraction technology for particle size determination. From the sieve analysis data in this case, it is difficult to assess the median particle size. However, this material can be classified as fine-grained, containing more than 50% of particles of <75µm.

A portion of the ladle slag of <63µm remaining from the initial sieving was ground by the ball mill of type *FRITSCH planetary mill pulverisette 5*. Each batch was milled at approximately 210 rot/min for 10 or 20 minutes by marble and steel balls. The resulting LS powder was analysed in the laboratory via laser diffraction technology, using samples from the 10- and 20-minute steel-milled ladle slag and the 20-minute marble-milled ladle slag.

The result of this analysis gives the particle size distributions pictured in Figure 3.

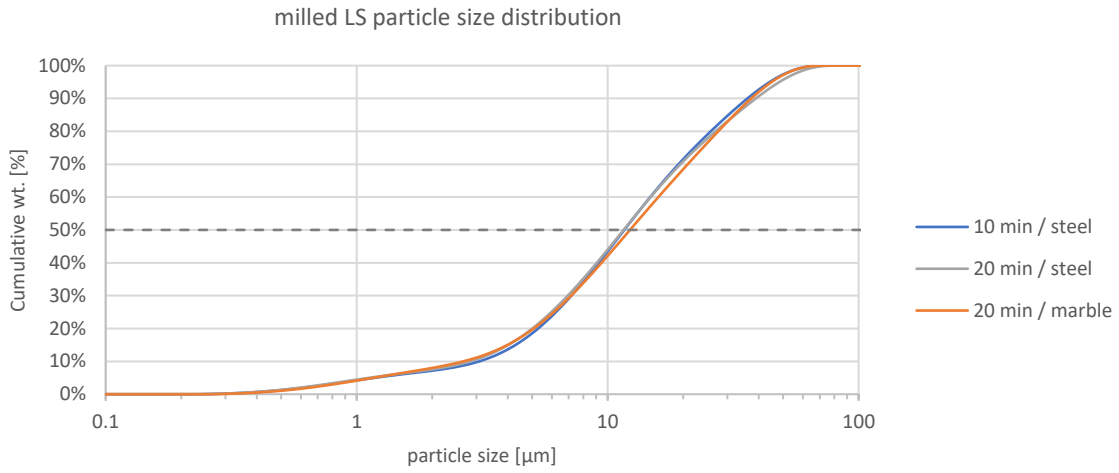

Figure 3: milled LS particle size distribution

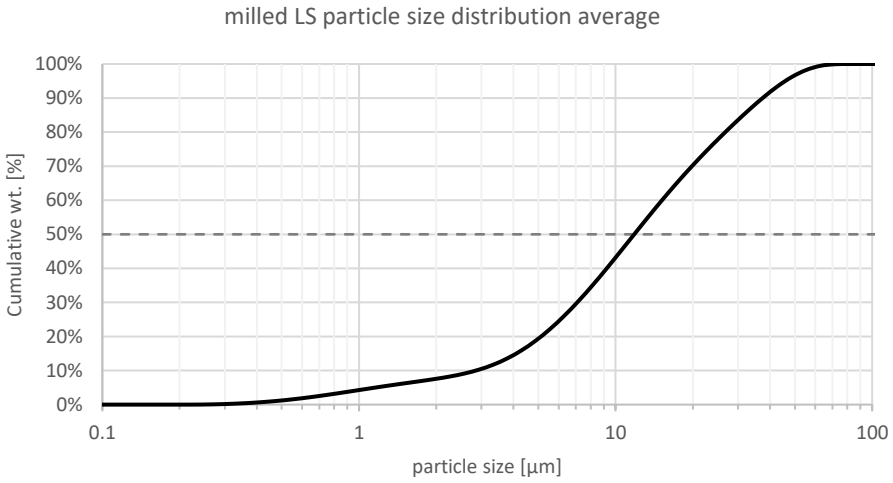

Figure 4: milled LS particle size distribution average

D_{50} = 11.8 µm

D_{10} = 2.89 µm

D_{60} = 15.4 µm

$$Uniformity\ coefficient\ C_U = \frac{D_{60}}{D_{10}} = 5.3$$

It can be concluded that the resulting powder is fine-grained and well-graded. The differences resulting from different times of steel milling are negligible. However, the marble-milled material showed slightly larger grain sizes compared to the steel-milled, which could also be assessed visually due to a darker shade of the resulting powder.

(II) De-S slag

For the particle size determination of the De-S slag, only one batch of 760g was analysed for research purposes. In the De-S slag, some smaller particles are typically loosely clustered in large agglomerates. Before starting the particle size measurement, these were ground down for up to 10 minutes by hand with light pressure, to ensure a more homogeneous material. This process was also followed when mixing and preparing samples for testing.

For particle size measurement, the following 7 sizes of sieves were used:

4mm – 1mm – 500µm – 250µm – 125µm – 106µm – 63µm

The material was passed through each sieve, starting with the largest sieve size to the smallest. The results are collected below in Table 1 and Figure 5:

Table 1: De-S slag particle size distribution

PARTICLE SIZE DISTRIBUTION	PARTICLE SIZE [MM]	NET WEIGHT [G]	PERCENTAGE	CUM.%
<63µm	63	32.44	4.27%	4.27%
63<x<125µm	125	18.85	2.48%	6.75%
125<x<250µm	250	81.1	10.67%	17.41%
250<x<500µm	500	165.72	21.79%	39.21%
500µm<x<1mm	1000	178.97	23.54%	62.74%
1mm<x<4mm	4000	257.13	33.82%	96.56%
>4mm	100000	26.17	3.44%	100.00%
total	-	760.38	100.00%	-

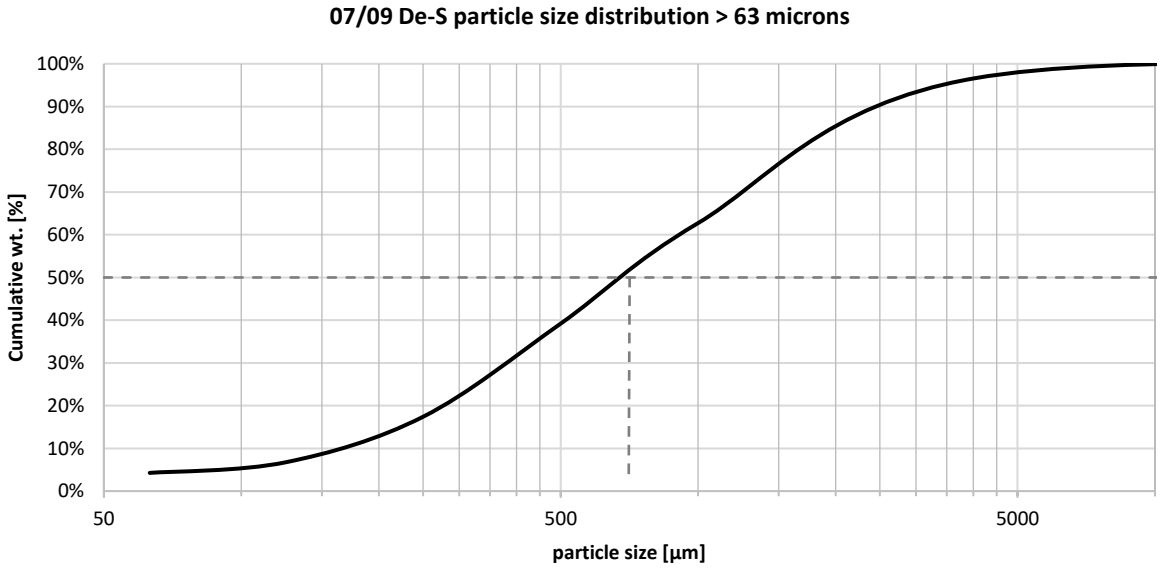

Figure 5: De-S slag particle size distribution

The De-S slag is of larger particle size than the ladle slag, resulting in a complete distribution using manual particle size determination.

From Figure 5, the following parameters were estimated:

D_{50} = 715 µm

D_{10} = 170 µm

D_{60} = 929 µm

$$Uniformity\ coefficient\ C_U = \frac{D_{60}}{D_{10}} = 5.5$$

As this slag is of large particle size with a very little fraction being below 75µm, we can conclude that this is a coarse-grained material. The uniformity coefficient indicates a well-graded material.

(III) Other materials

The BOF slag was not analysed for particle size distribution as its use was discontinued after a few samples. The particle size distribution of Portland cement used in later experiments is known, the material classified as fine-grained and well-graded. A representative PSD for OPC is shown in Figure 6 based on measurements by (Yoon, et al., 2015).

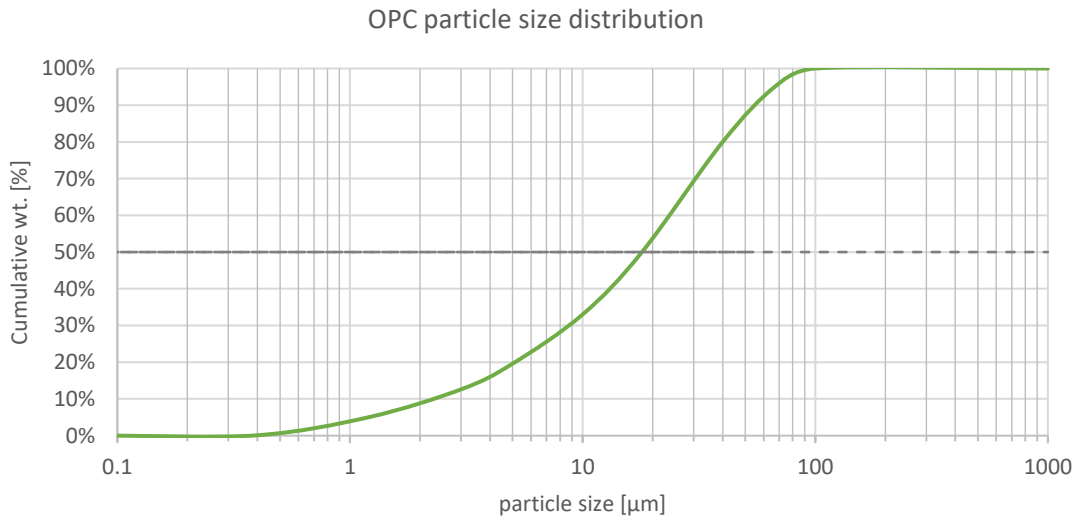

Figure 6: Portland cement, particle size distrubution

D_{50} = 18 µm

D_{10} = 2.2 µm

D_{60} = 22 µm

$$Uniformity\ coefficient\ C_U = \frac{D_{60}}{D_{10}} = 10$$

6.2 Material preparation

Before mixing, the ladle slag is milled to achieve smaller particle size. The aggregate slags are carbonated and hydrated before use.

(IV) Ladle Slag

The milled and unmilled LS was sorted into plastic bags by particle size and used in different configurations for the test samples.

The chemical composition of ladle slag is shown in Table 2 and is consistent with ladle slag composition in literature (Yildirim & Prezzi, 2011). Overall, the main constituents of ladle slag are CaO, Al_2O_3 and SiO_2. The high percentage of Al_2O_3 has to do with the steel slag being a byproduct of the steel refining process, when aluminium alloy is added in the production.

Table 2: chemical composition of ladle slag

Material	Element/Oxides (%, w/w)						
	CaO	MgO	Al_2O_3	SiO_2	SO_3	Fe_2O_3	TiO_2
Ladle Slag	50.6	3.8	24.4	13.9	0.40	0.40	4.1

(V) BOF and De-S slags

Two types of aggregate slags were prepared and used during experiments. BOF or blast oxygen furnace slag, and De-S slag, a by-product from the desulfurization process in steelmaking.

The aggregate slag was prepared in Finland with the aim to capture CO_2. This was done by carbonating this aggregate at 40°C in ambient pressure with CO_2 concentration of 20% for 48 hours. Before the carbonation process, particles of >2mm were removed from the slag.

The material formed large, loose agglomerates of up to 5cm in diameter, which were broken up manually before using the material for sample preparation. The BOF slag was used for several initial samples, however the majority of experiments were conducted using De-S slag. The De-S slag was noticeably more humid than the BOF slag, which was noticeable to the naked eye by a darker colour of the raw material, and a wetter solution of the final composite mix.

The chemical composition of the slags was evaluated in the laboratory at Oulu University and is summarised in Table 3. Similarly to steel slag, the main constituents are CaO and SiO_2. However, BOF slags also contain a high fraction of Fe_2O_3 which is a result of this slag being a by-product of iron-to-steel conversion, rather than the steel refining process.

On the next page, the table for chemical composition is given and the raw De-S slag is pictured before mixing.

Table 3: chemical composition of aggregate slags

Material	Element/Oxides (%, w/w)					
	CaO	MgO	Al_2O_3	SiO_2	SO_3	Fe_2O_3
De-S	55.40	1.64	2.15	15.19	4.98	16.06
BOF	54.59	1.86	1.15	12.99	0.18	21.35

Figure 7: De-S slag close-up

6.2 Mixing Process

To create the samples, the following different types of material combinations and preparation were used:

- Ladle slag and BOF mix (LS+BOF) *[4 samples]*

This was the initial recipe suggested by the University of Oulu. The samples were prepared from the ladle slag and BOF and mixed with gypsum and citric acid to increase workability time. Due to this being the first batch of testing, many experiments did not work out due to demoulding issues and very quick hardening of the material. Only 4 samples of this composition were subsequently tested.

- Ladle slag and De-S mix (LS+De-S) *[3 samples]*

Instead of BOF, De-S type slag was used as aggregate. This slag was noticeably wetter than the BOF, and some samples were damaged due to humidity-induced cracking. In total, only 3 samples were tested in uniaxial compression.

- OPC (CEM I 42.5 MPa or 52.5 MPa) and De-S (OPC+De-S) *[20 samples]*

After a series of poor results and careful consideration, the ladle slag was replaced with conventional cement to harden the material. 3 samples were made using 42.5 MPa cement, while the remaining 17 samples were made using 52.5MPa cement.

- OPC 52.5 MPa, De-S and ladle slag (OPC+De-S+LS) *[3 samples]*

Finally, 3 samples were made using an experimental mixture of OPC 52.5 MPa, De-S slag and low-particle size ladle slag.

(I) Ladle Slag and BOF mix (LS+BOF)

The composition of the LS+BOF mix is as follows, by weight percent:

MIX by wt%	BOF slag	Ladle slag	Gypsum	Citric Acid	Water
	72.5%	12.9%	5.5%	0.1%	9%

The ladle slag was prepared as a mix of particle sizes which were previously sieved/milled and stored by particle size. In total, more than 10 samples using LS+BOF mix were prepared, of which only 4 were tested, due to errors in the preparation and issues with demoulding.

The composition of the useful samples is collected in Table 4 below.

Table 4: composition of LS powder by sample (LS+BOF)

Sample	LS milled [%]		LS unmilled <63 [%]	LS >63 [%]	LS>106 [%]	LS>125 [%]
	Steel milled	Marble milled				
S01 – 26/04	30	30	10	20	5	5
S02/03 – 23/05	32.5	32.5	10	15	5	5
S04 – 24/05	32.5	32.5	17.5	3.5	7	7

Figure 8 shows the approximate particle size distribution curve compared to the slag prepared in Oulu. It is worth noting that the median particle size is around 12µm for the slag prepared in Oulu, while the median particle size for the slag prepared in Milan is slightly higher at 23-29µm. This is a limitation due to the milling equipment available.

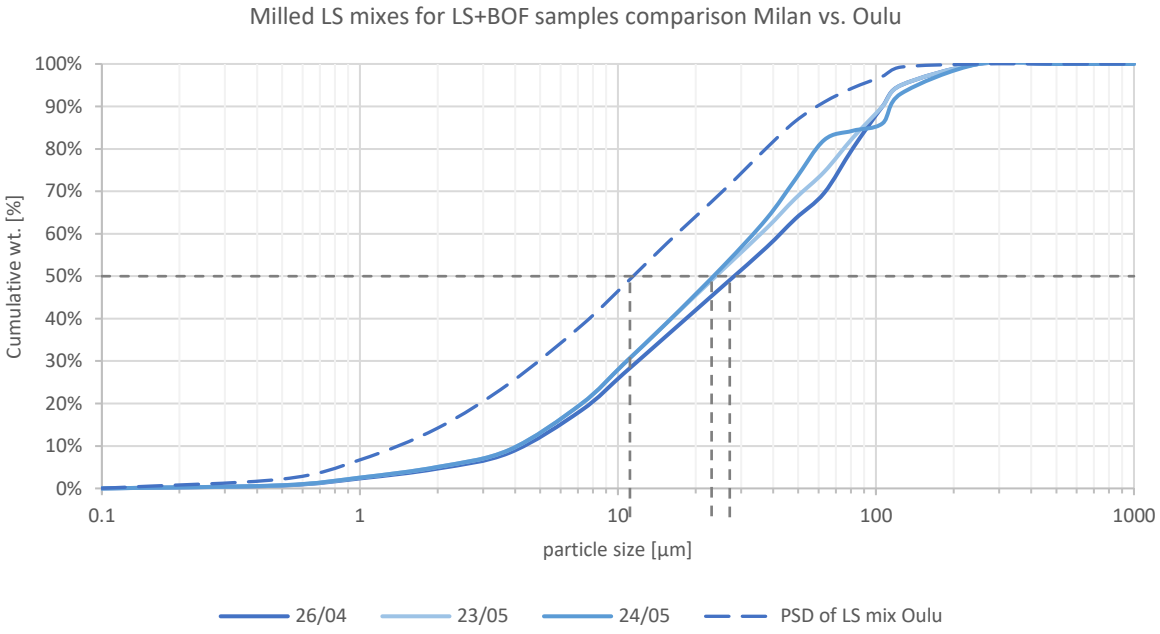

Figure 8: milled LS mixes for LS+BOF samples

As evidenced in Figure 8, the ladle slag mix (24/05 in particular) has some particle sizes missing in the mix (gap graded). Overall, the sample is fine-grained. In Table 8, the estimated grading parameters are collected, indicating a significant range of particle size with values consistently >8.

Table 5: grading parameters

parameters	26/04	23/05	24/05
D_{10}	4.3	4	4
D_{60}	42.5	35.5	33.3
$C_U = D_{60}/D_{10}$	9.9	8.9	8.3

After mixing of the ladle slag, the sample mix is prepared for casting in the following steps:

1. Gypsum is weighed and mixed into the ladle slag by hand.
2. In a separate bowl, the citric acid is mixed into the water until fully dissolved.
3. The citric acid in water is added into the ladle slag and gypsum mix. After about 2-3 minutes of mixing, a homogeneous paste should be obtained.
4. The dry BOF slag is added into the paste and mixed for 10 minutes using hands and a mechanical mixer.

(II) Ladle slag and De-S mix (LS+De-S)

The composition and mixing procedure of these samples is the same as before, with the BOF replaced by De-S slag:

MIX by wt%	De-S	Ladle slag	Gypsum	Citric Acid	Water
	72.5%	12.9%	5.5%	0.1%	9%

The same LS distribution is used as prepared before, with C_U = 8.3 and median particle size of around 24µm.

Table 6: composition of LS powder by sample (LS+DeS)

Sample	LS milled [%]		LS unmilled <63 [%]	LS >63 [%]	LS >106 [%]	LS >125 [%]
	Steel	Marble				
S05 – 11/06	32.5	32.5	10	15	5	5
S29/30 – 30/07	32.5	32.5	10	15	5	5

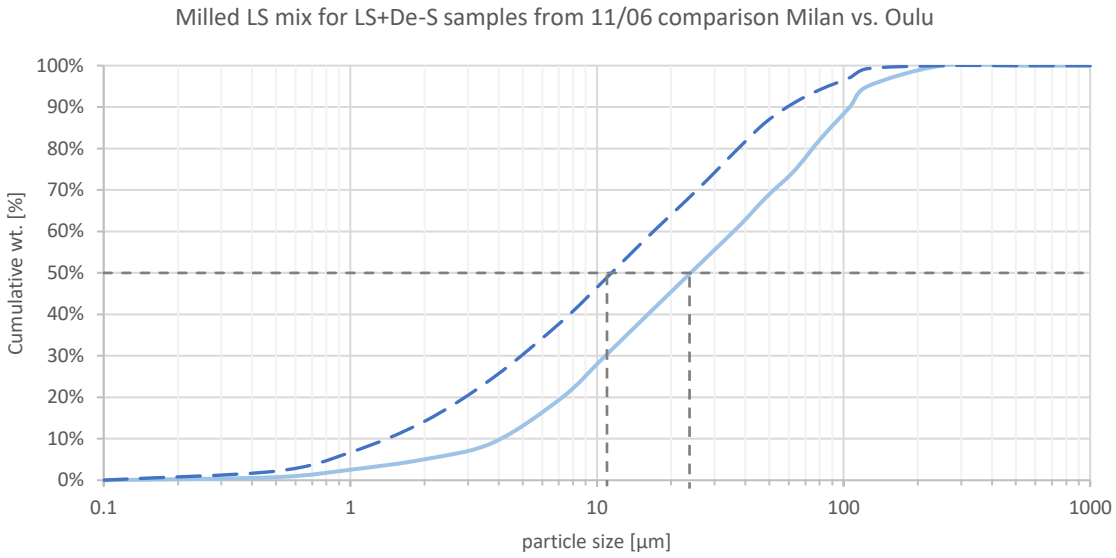

Figure 9: milled LS mixes for LS+DeS samples

(III) OPC (CEM I 42.5 MPa or 52.5 MPa) and De-S (OPC+De-S)

The new mixture was prepared in the following way:

MIX by wt%	De-S	CEM 42.5/52.5	Water
	82%	9%	9%

The mixture was prepared in the following steps:

1. The water and cement are weighed and mixed to obtain a homogeneous liquid.
2. The De-S slag is added to the mix and combined well for 10 minutes. As before, larger agglomerates in the De-S slag are broken up manually to achieve a homogeneous aggregate before mixing.

(IV) OPC 52.5 MPa, De-S and ladle slag (OPC+De-S+LS)

The composition of the OPC+De-S+LS mix is approximately as follows, by weight percent:

MIX by wt%	CEM 52.5	Ladle slag	De-S	Citric Acid	Water
	4.5%	9.1%	77.2%	0.1%	9.1%

This experimental mix contains predominantly fines of the ladle slag, with particle size <106µm exclusively. The resulting median size is 17.1µm and C_U = 6.66, both significantly lower than in the samples seen previously.

The LS particle size distribution is as follows:

Table 7: composition of LS powder by sample (OPC+DeS+LS)

LS milled [%]		LS unmilled <63 [%]	LS >63 [%]	LS>106 [%]	LS>125 [%]
Steel milled	Marble milled				
40	40	15	5	0	0

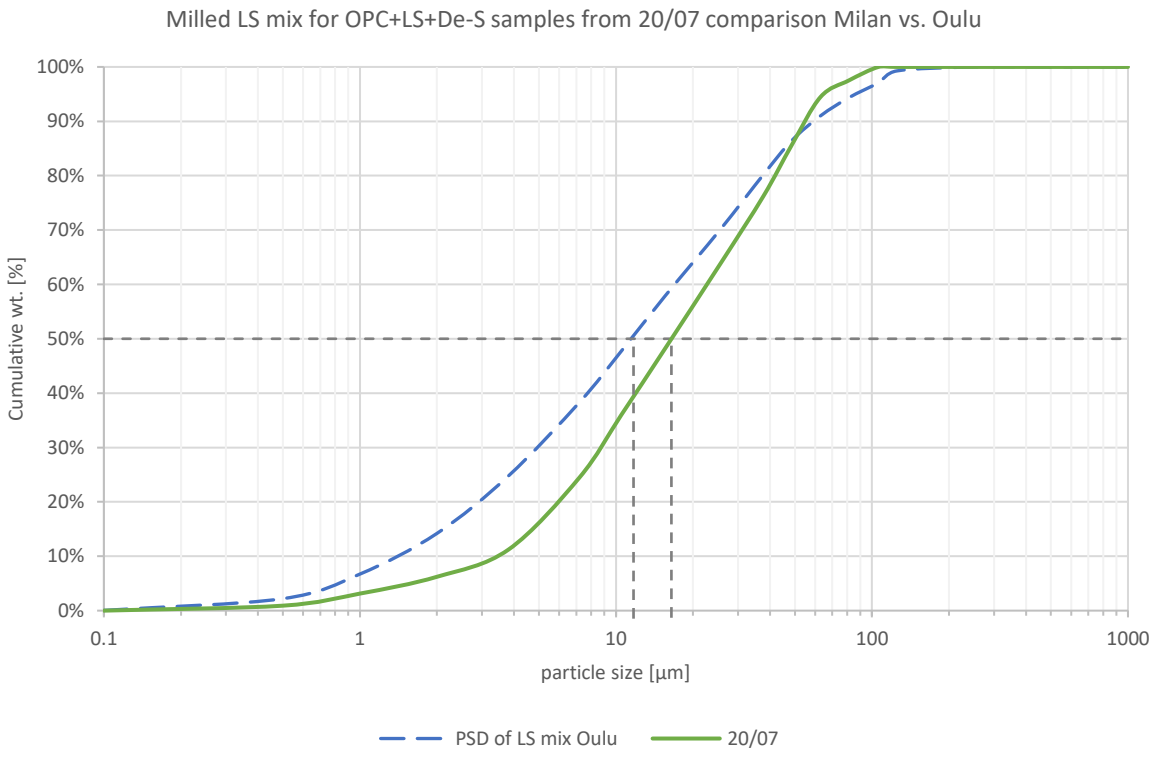

Figure 10: milled LS mixes for OPC+DeS+LS samples

After mixing of the ladle slag, the sample mix is prepared for casting similarly to the initial mix in the following steps:

1. The OPC is weighed and mixed into the ladle slag by hand.
2. In a separate bowl, the citric acid is mixed into the water until fully dissolved.
3. The citric acid in water is added into the OPC and ladle slag mix. After about 2-3 minutes of mixing, a homogeneous paste should be obtained.
4. The De-S slag is added into the paste and mixed for 10 minutes using hands and a mechanical mixer.

6.3 Casting

After producing each mixture, hollow steel cylinders of 54mm internal diameter were prepared for the casting of the samples. Several different approaches were taken for demoulding, such as attaching Teflon on the inside and using openable cylinders. These approaches failed, as the material would still adhere to the surface and it was impossible to remove the sample without damage (Figure 11). Eventually, the use of demoulding agents such as silicone/PTFE spray and demoulding oil were adopted and proved successful.

Typically, the inside of each cylinder was sprayed or oiled with demoulding agent in two layers, letting the first layer dry out before applying the second for maximum effect.

After placing the cylinders on a steel plate, the sample mixture was poured inside and compacted by hand, using a cylindrical metal tamper of similar diameter. Typically, 3 cylinders were used for the casting of approximately 1kg of sample mix.

Each specimen was compacted by an Instron 1185 testing machine at 10MPa. The specimens are cylindrical with the force applied on the circular top surface of 22.9 cm^2 area. Hence, up to 23 kN load was applied for sample compaction.

6.4 Curing

The specimens were typically demoulded within 24 hours of casting and placed in plastic bags at room temperature (20-25°C) to prevent moisture loss for at least 7 days. This allows the hydration reaction to progress and increase the strength of the material. Some samples were cured in a higher humidity environment, which was achieved by sealing them in a box with a small water container.

Figure 11: failed demoulding and high humidity curing attempts

7. Testing procedure

7.1 Compression test

Uniaxial compression tests were performed using an electromechanical INSTRON model 1185 testing machine (Figure 12) with a load cell of 100kN. The specimens used in this analysis were cylindric, 5.4 cm in diameter and of 93mm length on average.

Irregularities on the surface of the samples typically occur due to casting, demoulding and eventual volume changes during curing. To ensure a sufficiently smooth and planar surface, the samples were cleaned of any loose particles and a self-aligning compression plate was used adopting a spherical hinge. The latter helps to recover uneven parallelism of the top and bottom surface of the specimen.

The testing method was set up in the Instron system to execute an automatic compression test by imposing a displacement increment rate of 1 mm/min. Before running the test, the specimens were wrapped using cling foil to contain any loosening fragments of the sample during testing. This does not affect the mechanical behaviour of the specimen.

Figure 12: INSTRON model 1185 and testing specimen

During each test, the force and the displacement were recorded by the machine. Using the compression test results, the compression strength (considering the initial area of the loaded surface), as well as the strain (adopting the specimen height as base length) were evaluated.

7.2 Thermo-gravimetric analysis

TGA analysis was conducted on 3 samples of the OPC 52.5 + De-S slag mixture (see chapter 6.2, section (III)) after 7, 36 and 56 days of curing, and one LS + De-S slag mixture (chapter 6.2, section (II)) after 7 days of curing to assess the degradation and mass loss of different phases in the material with increasing temperature.

The analysis was conducted using the TA Instruments Q500 Thermogravimetric analyser and a platinum sample pan.

The experimental process is conducted in the following way:

1. After taking a small material sample from the specimen, it is weighed on the tared sample pan.
2. The TGA furnace housing is lowered and fixed over the sample.
3. The sample is ramped at 10.00 °C/min from room temperature to around 1000°C (see Figure 13).
4. At max. temperature, the sample is left in isothermal condition for 5 minutes.
5. The apparatus is cooled off to room temperature and purged with nitrogen and pressurized air post-experiment.

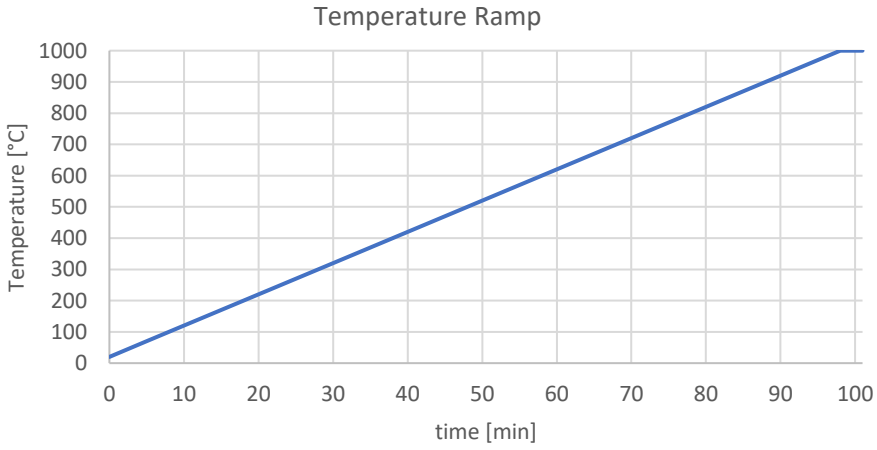

Figure 13: TGA temperature ramp

7.3 Freeze-thaw test

To investigate the durability of our material, 5 samples of the OPC 52.5 + De-S slag mixture (see chapter 6.2 section (III)) were subjected to freeze-thaw cycles under extreme conditions. The procedure adopted for this experiment is following the recommendation by (Setzer, et al., 1996). In total, the specimens underwent 28 freezing-thawing cycles of 12 hours each (see Figure 14) and 1 week of pre-soaking in a testing liquid in the beginning and after 14 cycles. This procedure is, despite being rather short, a very severe test due to several factors: the pre-saturation reduces any possible air entrainment, which is associated with higher resistance; the extreme cycles of 20 to -20°C are not commonly found in real-life applications; the use of de-icing solution with 3% is the worst possible condition according to (Valenza II & Scherer, 2007). The procedure is approximately consistent with the Eurocode conform process outlined in CEN/TS 12390. While the standard recommends up to 56 cycles, 28 cycles are sufficient in this case for preliminary testing, as well as for standard testing for the application of paving blocks.

Pre-saturation of specimens will be done using the following liquids:
- distilled water (3 samples)
- de-icing agent solution with 97% by weight of distilled water and 3% by weight of NaCl (2 samples)

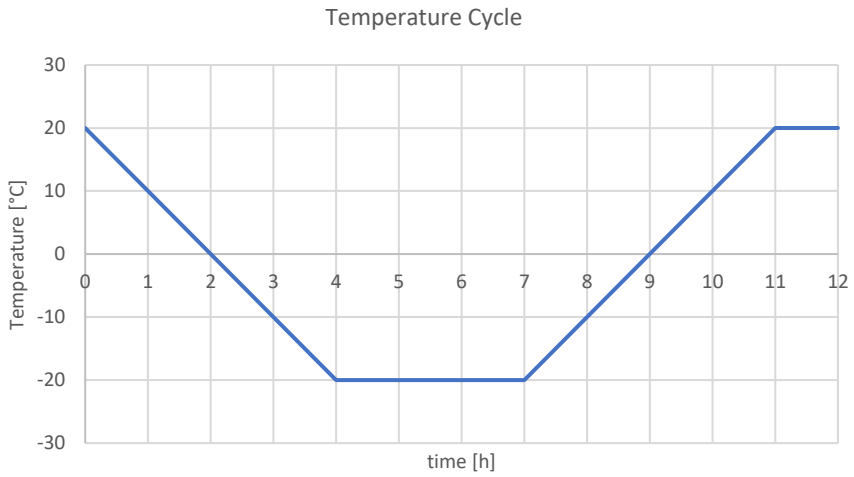

Figure 14: temperature ramp FT cycling

The temperature is cycled in 12-hour intervals, where it is lowered from 20 to -20°C in 4 hours at a constant heating rate, maintained at -20°C for 3 hours, and heated again in 4 hours to 20°C where it is maintained for 1 hour.

The testing process is conducted in the following steps:

1. Measurement of specimen dimensions and weight.
2. Lateral sealing of specimens using PARAFILM© tape to avoid any liquid penetrating the material from the side. The sealed specimens are labelled and placed in the container as pictured in Figure 15.
3. 1 week pre-saturation of sample. To allow saturation from the bottom surface of the specimen, it is propped up and placed in a closed container filled with testing liquid, keeping the top of the sample dry, as pictured in Figure 15.
4. 14 freezing-thawing cycles.
5. Measurement of specimen dimensions and weight.
6. 1 week of pre-saturation as before.
7. 14 freezing-thawing cycles.
8. Measurement of specimen dimensions and weight.

After the specimens are air-dried, any flakes and scaling on the surface is removed and weighted. If the samples retain any strength, a compression test is conducted as before. The results expected from this are the compressive strength, volume and density changes and scaling resistance.

Figure 15: specimens pre-saturation

8. Results

In total, over 50 specimens of 5 different types were prepared in the scope of this research project. 30 specimens were of good enough quality to be tested for compressive strength and 6 more samples were tested for durability.

8.1 Ladle Slag Based Samples (LS+BOF, LS+De-S)

Overall, the initial sample material (see LS+BOF, chapter 6.2) performed poorly. The workability of the LS+BOF samples was very sensitive, as shown from trial mixtures with different relative amounts of citric acid. Reducing the percentage of CA from around 0.5% to <0.2% showed significant variations in setting time.

CA	0.46%	0.35%	0.23%	<0.2%
setting time	>60 min	>60 min	45 min	<15 min

To explore the effect of humidity, two samples were partially cured in a humid environment, where the specimen was placed in a sealed box with a small water-filled container.

Ladle slag + BOF	casted	Dry curing	Hum. curing	condition
Specimen A	24/05/2021	9 days	7 days	Very cracked
Specimen B	31/05/2021	2 days	7 days	Slightly cracked

Both samples were cured in humid conditions for 7 days and deteriorated in the process, with sample A showing more damage than sample B (Figure 16). Since sample A was pre-cured in dry conditions for 9 days, it likely gained higher initial strength compared to sample B, that pre-cured for 2 days only. Hence, sample A may have developed more cracking due to stronger internal bonds, while sample B was able to accommodate more expansion. Nevertheless, both specimens were easily crushed by hand and curing in high humidity was deemed unsuitable for further experiments with this material.

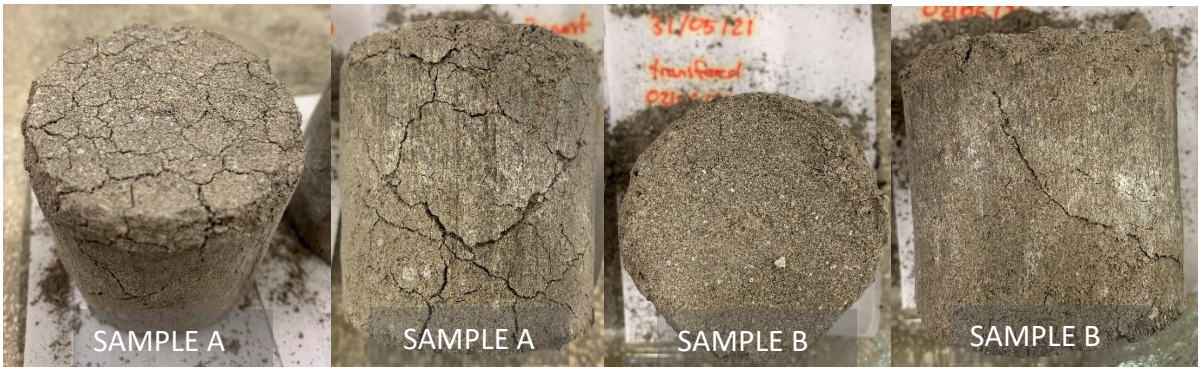

Figure 16: samples A and B post high humidity curing

4 specimens were tested under uniaxial compression with details and results summarised in Table 8. For one sample, the median particle size of the LS was slightly lower, which had no apparent effect on the material strength.

Table 8: LS+BOF specimens results

sample	description	casted	opened	tested	cured	max. load P	c. strength f_{ck}
					[days]	[kN]	[MPa]
S01	LS+BOF	26/04	11/05	31/05	15	7.07	3.09
S02	LS+BOF	23/05	31/05	31/05	8	4.57	1.99
S03	LS+BOF	23/05	31/05	31/05	8	3.90	1.70
S04	LS+BOF	24/05	02/06	02/06	9	3.58	1.56

The compressive strength development for the LS+BOF samples was very low, with a maximum value of 3.09 MPa after 15 days of curing. Slightly higher strength can be expected for longer curing time, however due to the poor initial results and the limited availability of the BOF slag at the time, the study of this material was discontinued.

The next set of experiments was conducted using carbonated De-S slag instead of BOF as aggregate. This mixture performed very poorly, with virtually no samples developing enough compressive strength to sustain load. The De-S slag mixture appears to have much higher water content compared to the BOF slag, with water escaping during compaction and darker-looking resulting samples. The hydration reaction of the mixture resulted in significant cracking and expansion of samples during humid curing, some expansion on few specimens during dry curing as well (Figure 17).

Figure 17: casting and curing of specimen

Overall, around 15 specimens were cast of this material, with curing time ranging from 7-33 days. 3 specimens were subsequently tested with details and results collected in Table 9.

Table 9: LS+DeS specimens results

sample	description	casted	opened	tested	cured	max. load P	c. strength f_{ck}
					[days]	[kN]	[MPa]
S05	LS+DeS	11/06	22/06	22/06	11	1.63	0.71
S29	LS+DeS	30/07	30/08	30/08	31	4.96	2.17
S30	LS+DeS	30/07	30/08	30/08	31	4.86	2.12

While strength gain was significant for samples between 11 and 31 days of curing, it can be concluded that this material is not suitable for any load-bearing application. Figure 18 shows the stress-displacement curve of each sample for LS+BOF and LS+DeS mix.

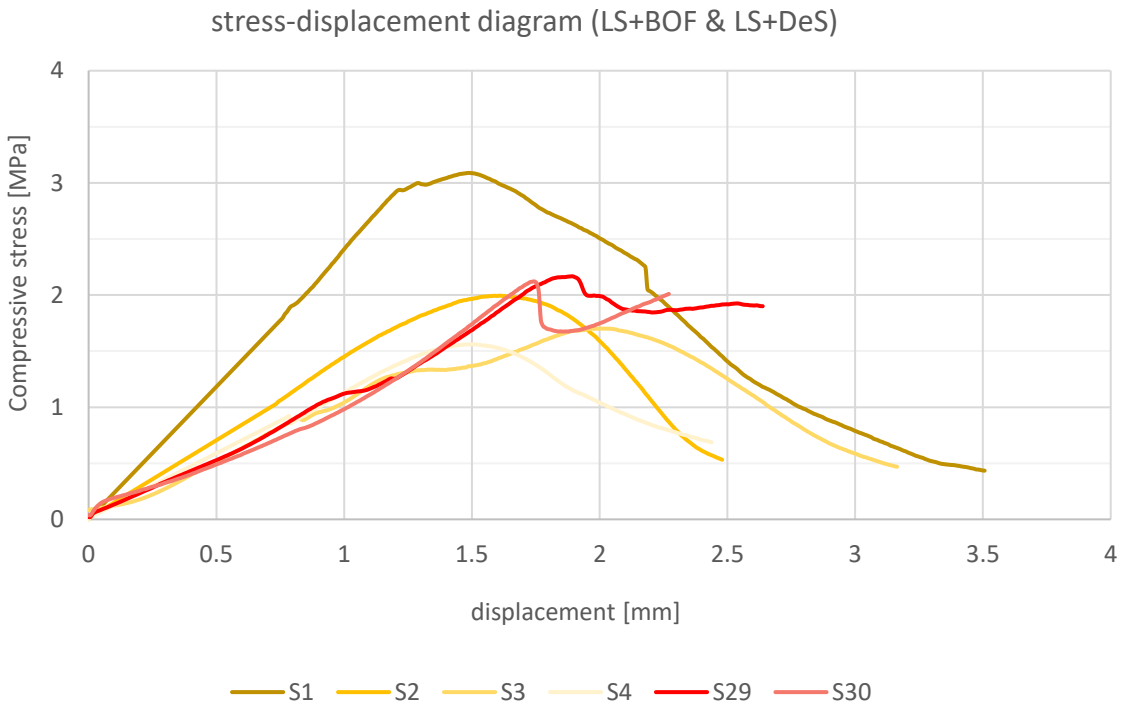

Figure 18: LS-based samples stress-displacement diagram

8.2 OPC Based Samples (OPC 42.5/52.5 and De-S)

Due to the poor performance of the initial material mixture, the ladle slag was replaced with conventional Portland cement. While this increased the environmental impact of the mixture, it did lead to significant strength gain of the samples.

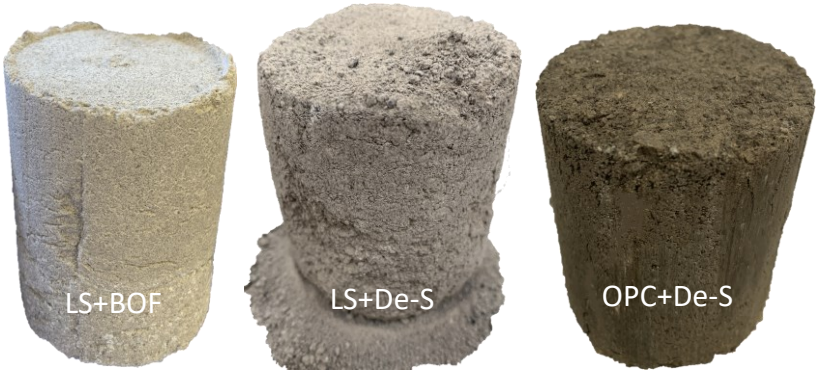

Figure 19: specimens of different material composition

8.2.1 Compression test

Compression tests were conducted on 17 samples in total. The samples were cured only in sealed conditions using plastic bags to avoid evaporation, for 7 to 56 days.

The details and compressive strength of each sample is reported in Table 10. The highest compressive strength was observed for specimen S16 (56 days of curing) with 14.22 MPa of sustained compressive stress at failure. Furthermore, specimen S11 (27 days of curing) and S28 (31 days of curing) reached peak stresses of 13.33 MPa and 13.02 MPa.

Table 10: OPC 52.5MPa + DeS specimens results

sample	description	casted	opened	tested	cured	max. load P	c. strength fck
					[days]	[kN]	[MPa]
S09	OPC52+DeS	30/06	27/07	27/07	27	18.81	8.21
S10	OPC52+DeS	30/06	27/07	27/07	27	23.64	10.32
S11	OPC52+DeS	30/06	27/07	27/07	27	30.53	13.33
S12	OPC52+DeS	02/07	20/07	20/07	18	22.44	9.80
S13	OPC52+DeS	02/07	20/07	20/07	18	20.88	9.12
S14	OPC52+DeS	02/07	20/07	20/07	18	28.41	12.40
S15	OPC52+DeS	05/07	30/08	30/08	56	25.74	11.24
S16	OPC52+DeS	05/07	30/08	30/08	56	32.57	14.22
S17	OPC52+DeS	05/07	30/08	30/08	56	26.62	11.62
S21	OPC52+DeS	21/07	28/07	28/07	7	15.48	6.76
S22	OPC52+DeS	21/07	28/07	28/07	7	15.58	6.80
S23	OPC52+DeS	21/07	28/07	28/07	7	10.83	4.73
S24	OPC52+DeS	27/07	30/08	30/08	34	27.55	12.03
S25	OPC52+DeS	27/07	30/08	30/08	34	24.57	10.73
S26	OPC52+DeS	27/07	30/08	30/08	34	21.70	9.47

S27	OPC52+DeS	30/07	30/08	30/08	31	27.37	11.95
S28	OPC52+DeS	30/07	30/08	30/08	31	29.81	13.02

Effect of L/d ratio

The l/d ratio of the cylindrical specimens tested in this experimental investigation is about 1.72 on average, which is slightly below the specified l/d value of 2 for standard testing methods for compressive strength specified in EN 206-1. To allow comparison between samples of different l/d ratios in terms of maximum compressive strength, the technical standard ASTM C42 provides a correction factor of specimen with l/d ratio ≤ 1.75.

$$f_{ck,cyl,corr} = f_{ck,cyl} * CF$$

For the specimens with an l/d ratio of <1.75, the maximum compressive strength was multiplied with the correction factor, which was interpolated from the values given in ASTM C42 section 9.1. The results are collected in Table 11.

Table 11: OPC 52.5MPa + DeS: l/d ratio and corrected results

sample	cured	c. strength fck	l/d	CF	corr. $f_{ck,cyl}$
	[days]	[MPa]	[-]	[-]	[MPa]
S09	27	8.21	1.72	0.98	8.03
S10	27	10.32	1.72	0.98	10.09
S11	27	13.33	1.72	0.98	13.03
S12	18	9.80	1.72	0.98	9.58
S13	18	9.12	1.72	0.98	8.91
S14	18	12.40	1.72	0.98	12.13
S15	56	11.24	1.76	1.00	11.24
S16	56	14.22	1.85	1.00	14.22
S17	56	11.62	1.76	1.00	11.62
S21	7	6.76	1.72	0.98	6.61
S22	7	6.80	1.72	0.98	6.65
S23	7	4.73	1.72	0.98	4.62
S24	34	12.03	1.59	0.97	11.64
S25	34	10.73	1.78	1.00	10.73
S26	34	9.47	1.64	0.97	9.20
S27	31	11.95	1.59	0.97	11.56
S28	31	13.02	1.62	0.97	12.62

Averages of the corrected compressive strength were evaluated for different curing times and compared in a histogram (Figure 20). The strength gain of the specimens is significant after 3-4 weeks, with a strength increase of about 75% between 1 and 4 weeks and doubling of strength after 56 days with respect to 7 days of curing.

This result indicates a very low initial strength. For conventional concrete, the 7-day strength should not be below 65% of the target 28-day strength, whereas for this composite, the strength reached after 7 days is only about 57% of the 27-day strength.

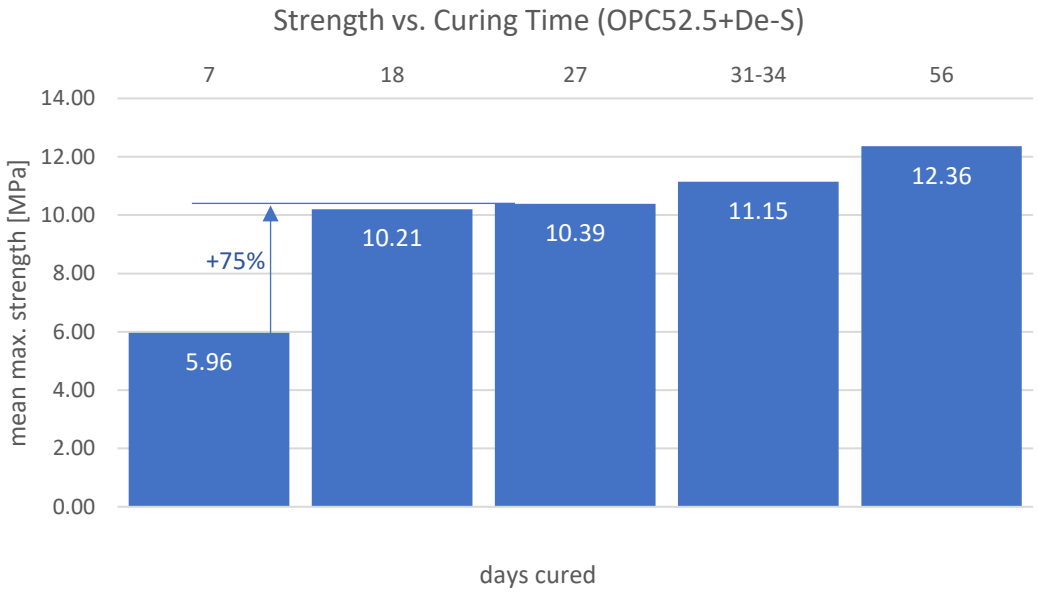

Figure 20: OPC 52.5MPa + DeS: strength vs. curing time histogram

Some trials were also conducted using OPC 42.5 MPa (S06-S08) as well as with OPC 52.5 MPa and re-introduction of ladle slag in smaller particle sizes (S18-S20). The exact composition can be found in chapter 6.2, sections (III) and (IV). However, the experiments were not continued for those configurations. For completeness, details and results are summarised in Table 12.

Table 12: OPC 42.5MPa + DeS and OPC 52.5MPa + DeS + LS specimens results

sample	description	casted	opened	tested	cured	max. load P	c. strength fck
					[days]	[kN]	[MPa]
S06	OPC42+DeS	24/06	02/07	02/07	8	14.10	6.16
S07	OPC42+DeS	24/06	02/07	02/07	8	18.65	8.14
S08	OPC42+DeS	24/06	02/07	02/07	8	16.23	7.09
S18	OPC52+LS+DeS	20/07	30/08	30/08	41	18.42	8.04
S19	OPC52+LS+DeS	20/07	30/08	30/08	41	23.61	10.31
S20	OPC52+LS+DeS	20/07	30/08	30/08	41	23.31	10.18

Stress-displacement diagrams for these specimens can be found in the Annex.

The laboratory test curve shows an almost linear behaviour of the material under compression before failure. To remove the initial effect of uneven parallel loaded surfaces of the specimen on the compression load-displacement curve, a linear approximation of the initial slope was fitted, and the origin re-calculated by subtracting the strain where the new linear slope crosses the x-axis.

In Figure 21, the approximations of the linear elastic slope of an OPC52.5+DeS test curve is depicted. The equation for each slope was determined by linear approximation.

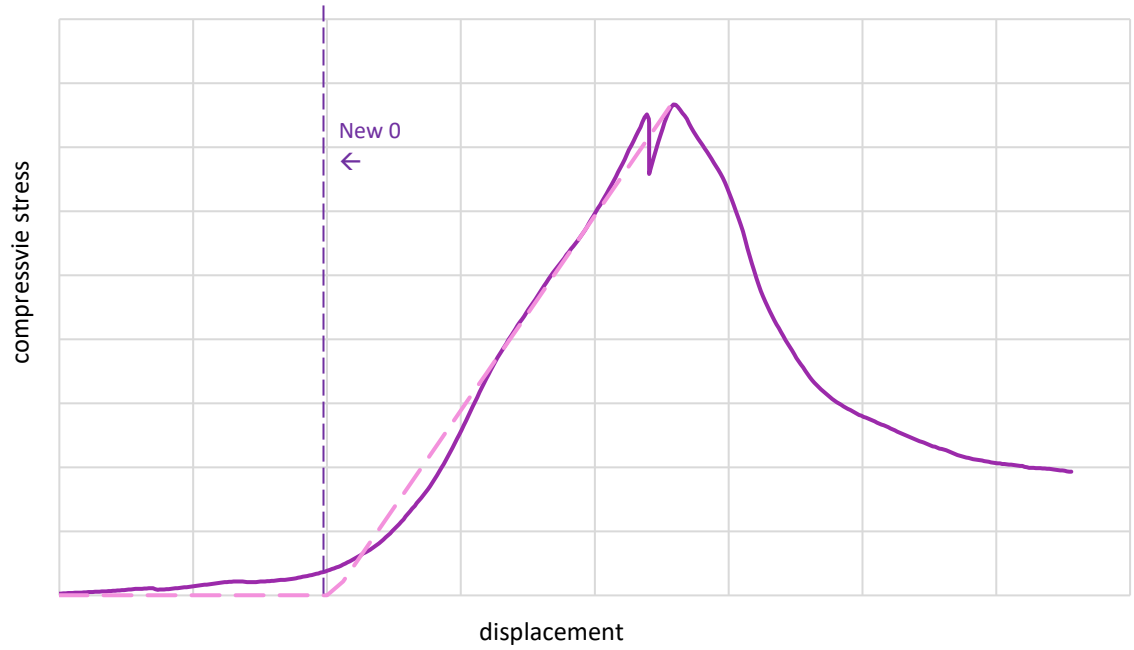

Figure 21: elastic curve fitting process

Finally, the modified stress-strain diagrams are depicted in Figure 22 – 25, grouping specimen by curing time. The specimen with curing time of 7 days were not considered due to the low strength.

Just like concrete, the composite is a brittle material. During the experiments, the composite behaves almost linearly elastic up to failure – unlike concrete, which typically has a slightly decreasing slope up until the peak load is reached. For the composite, the initial slope can be modelled as constant, elastic, with deviation from the linear behaviour just slightly before failure. This is due to small, stable cracks starting to form, that are however still capable of supporting some load increase, which was observed during the experiment. The relatively small amount of plastic deformation before failure implies a more immediate, brittle failure. After the material reaches peak load, the composite typically exhibits strain-softening

behaviour. In very few cases, a load plateau/short “plastic” range was observed, which however could be due to inhomogeneities of the specimen surface and cracking during failure.

In general, stress-strain curves are subject to many factors. Research suggests that bigger specimens can exhibit a more rapid failure or fracture compared to smaller samples (size effect), which tend to fail by “plastic” collapse (Carpinteri & Ingraffea, 1984). Material homogeneity, which is affected by proper mixing during preparation, can also have a significant effect on the failure mechanisms, especially due to differences in crack propagation. Additionally, the strength of the specimens can be affected by initial defects that could have occurred due to demoulding, or potentially, volume changes during curing. This is often the reason for variations in the stress-strain curve of nominally identical samples.

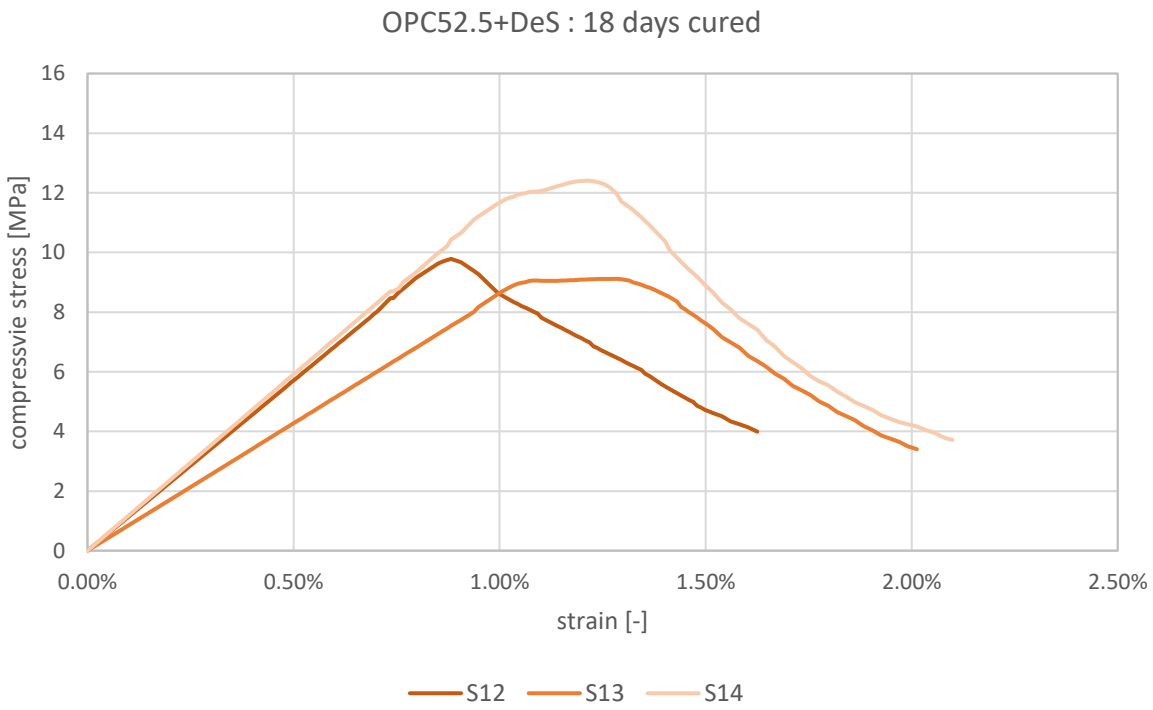

Figure 22: OPC52+DeS: 18 days stress-strain diagram

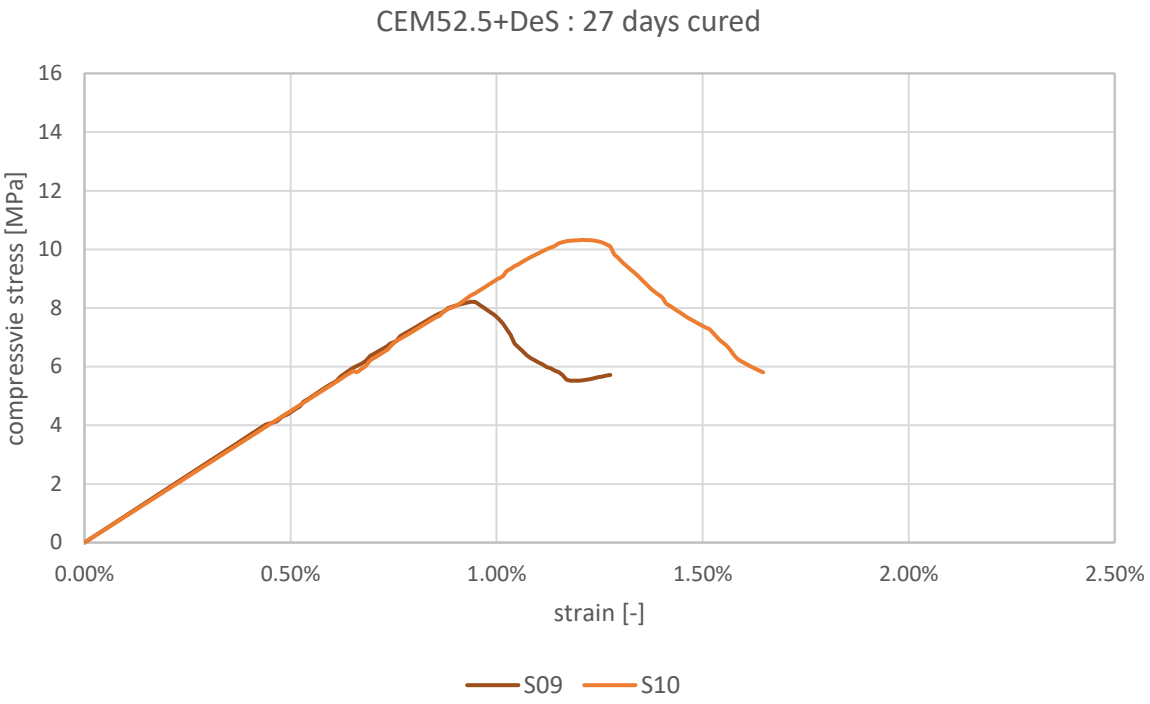

Figure 23: OPC52+DeS: 27 days stress-strain diagram

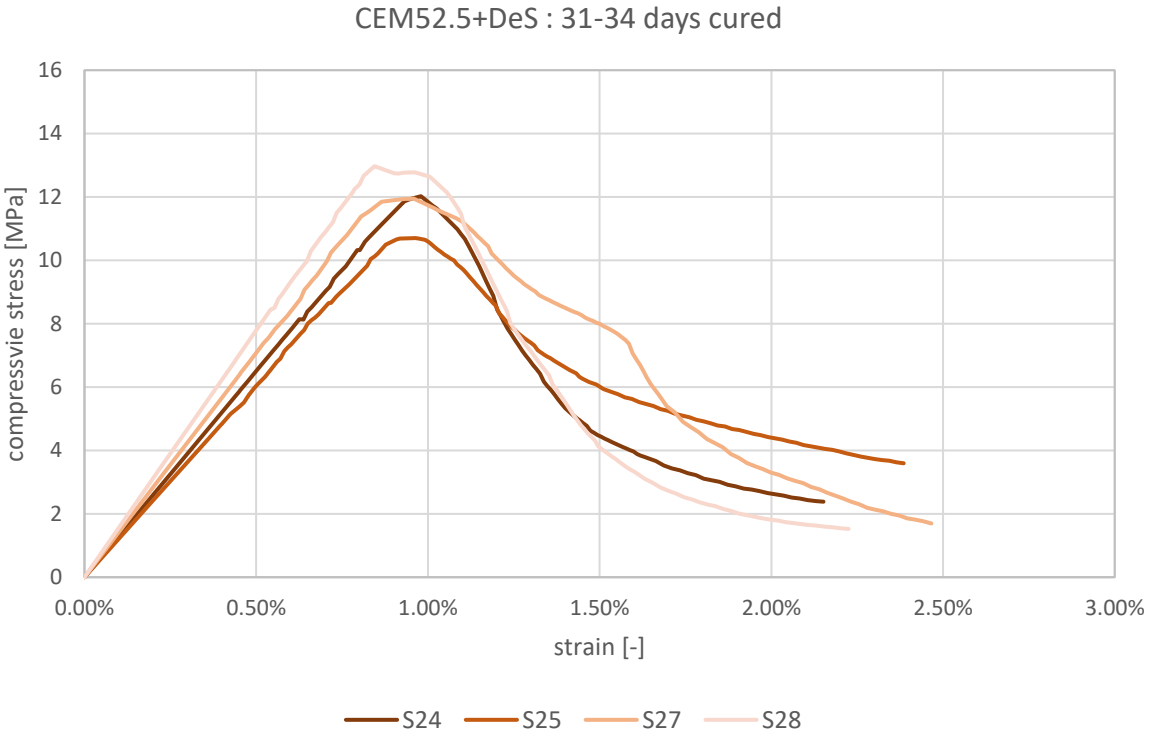

Figure 24: OPC52+DeS: 31-34 days stress-strain diagram

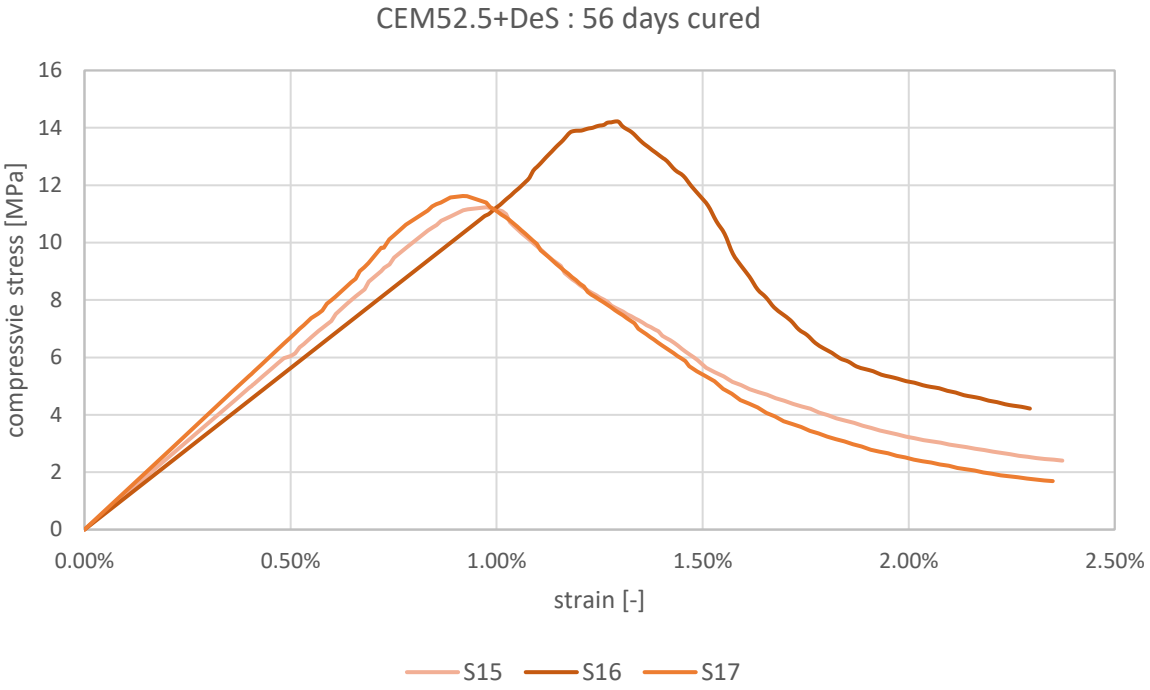

Figure 25: OPC52+DeS: 56 days stress-strain diagram

Post-peak behaviour

Post-peak stress-strain behaviour is very variable, as it depends on several external factors, mainly relating to the geometry and boundary conditions of the specimen, as well as load control and sensitivity of the testing machine (Bineshian, 2014). In the case of steady loading, the fracture occurs almost immediately after peak load is reached. Since this analysis was conducted using a controlled displacement rate, the material is subjected to a decreasing load after the peak, so plastic collapse and strain-softening occurs instead of brittle fracture.

Within these boundaries, post-peak behaviour is generally influenced by how the aggregates fail in the material. After the initial failure caused by cracking at the aggregate-cement boundaries, the aggregate fails in the post-peak range.

Overall, the post-peak curves do not vary significantly among the specimens. The results indicate strong aggregates and high fracture energy compared to conventional concrete and OPC-based mortar, such as the one pictured in Figure 26.

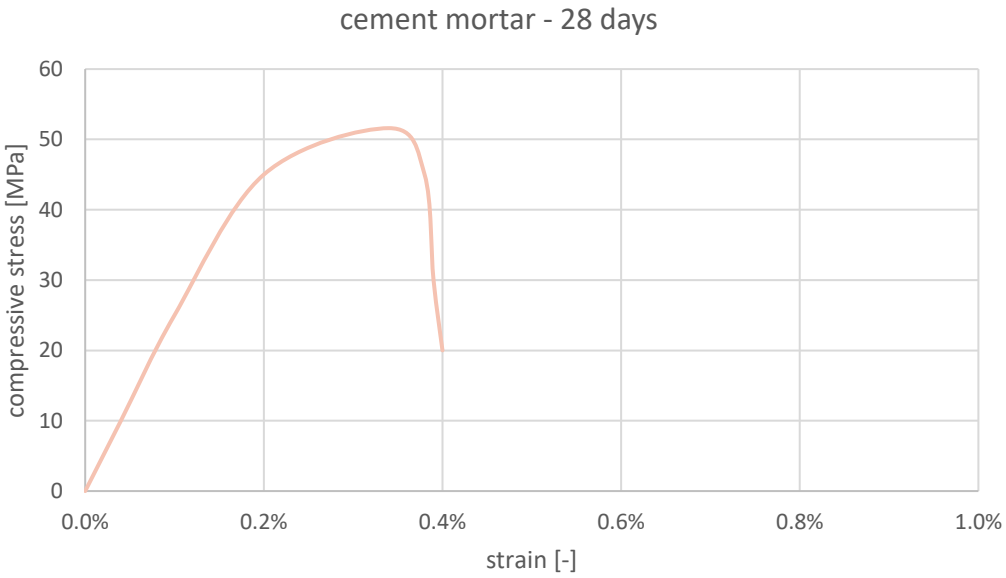

Figure 26: cement mortar: stress-strain diagram (Lima, et al., 2014)

Elastic Modulus

Assuming a homogeneous material, the elastic moduli of the OPC52.5+DeS samples were evaluated. The elastic modulus or Young's modulus, is characterised as the slope of the initial elastic branch of the curve. The elastic modulus is calculated as the ratio of stress applied to the material to the strain caused and is derived from Hooke's Law:

$$\sigma = E * \varepsilon$$

Higher-strength mortar has an elastic modulus which is often comparable to conventional concrete (Arash, 2012). Some standards recommend values to estimate the elastic modulus of concrete as a function of characteristic compressive strength:

$$\text{Per ACI } 318-08: \quad E = 4700 * \sqrt{f_{ck}}\ [MPa]$$
$$\text{Per EN } 1992\text{: } 1: \quad E = 22 * [(f_{ck,mean})/10]^{0.3}\ [MPa]$$

However, for weaker OPC-based mortar such as the one tested by (Zeng, et al., 2016), the elastic modulus has the following approximate correlation with strength:

$$E^* = 125 * f_{ck}\ [MPa]$$

The values (actual and estimated from the equation for E*) for the elastic modulus of each OPC52.5+DeS specimen are summarised in Table 13 by curing time.

Table 13: OPC52+DeS: strains and elastic modulus E

sample	description	cured	c. strength f_{ck}	strain at f_{ck} ε_{fck}	predicted E	actual E*	mean E
		[days]	[MPa]	[%]	[GPa]	[GPa]	[Gpa]
S21	OPC52+DeS	7	6.76	0.86%	0.84	1.15	
S22	OPC52+DeS	7	6.80	0.76%	0.85	1.14	1.03
S23	OPC52+DeS	7	4.73	0.85%	0.59	0.79	
S12	OPC52+DeS	18	9.80	0.88%	1.22	1.14	
S13	OPC52+DeS	18	9.12	1.29%	1.14	0.85	1.06
S14	OPC52+DeS	18	12.40	1.21%	1.55	1.18	
S09	OPC52+DeS	27	8.21	0.94%	1.03	0.91	
S10	OPC52+DeS	27	10.32	1.21%	1.29	0.90	1.17
S11	OPC52+DeS	27	13.33	0.80%	1.67	1.70	
S27	OPC52+DeS	31	11.95	0.96%	1.49	1.42	
S28	OPC52+DeS	31	13.02	0.84%	1.63	1.56	
S24	OPC52+DeS	34	12.03	0.98%	1.50	1.30	1.40
S25	OPC52+DeS	34	10.73	0.96%	1.34	1.21	
S26	OPC52+DeS	34	9.47	0.70%	1.18	1.53	
S15	OPC52+DeS	56	11.24	0.98%	1.41	1.23	
S16	OPC52+DeS	56	-14.22	1.29%	1.78	1.13	1.23
S17	OPC52+DeS	56	-11.62	0.93%	1.45	1.34	

As evident from Table 13, the modulus of elasticity is similar to the one estimated based on research on OPC-based mortars (Zeng, et al., 2016). It is evident from both the stress-strain diagrams and Table 13, that the strains at peak are high, ranging from 0.8 to values as high as 1.3%. This is relatively high compared to conventional concrete and some mortars, where strains at peak typically do not exceed 0.5%.

The low modulus may be due to the low density of the composite. With just above 2000kg/m^3, the material is on the upper limit for values for lightweight concrete, which is often associated with higher deformations.

The low values of E indicate that the material cannot withstand very high stresses, however it is able to deform relatively easily compared to conventional concrete. Low elastic modulus is undesirable in terms of serviceability, depending on the application.

8.2.2 Failure Mode

The specimens tested under compression form cracks along the surface which give information about the failure mode. The samples were assessed visually and compared to the compression test typical fracture chart from the ASTM C39.

In general, the specimens exhibit similar types of fracture pattern, which is pictured in Figure 28. In almost all cases, vertical cracks form along the sample surface, suggesting fracture pattern of type 3. Most samples also exhibit cracking and loosening at the top surface perimeter, less frequently also at the bottom surface (Types 5 and 6). This suggests that the specimens were typically not sufficiently well formed and homogeneous. However, some specimens exhibit fracture patterns of type 2, suggesting a partially well-formed cone.

This is likely due to slight inconsistency during casting, where a steel cylinder of slightly smaller diameter than the specimens was used for compaction. This could result in an uneven pressure distribution during compaction, as well as an uneven top surface of the specimens.

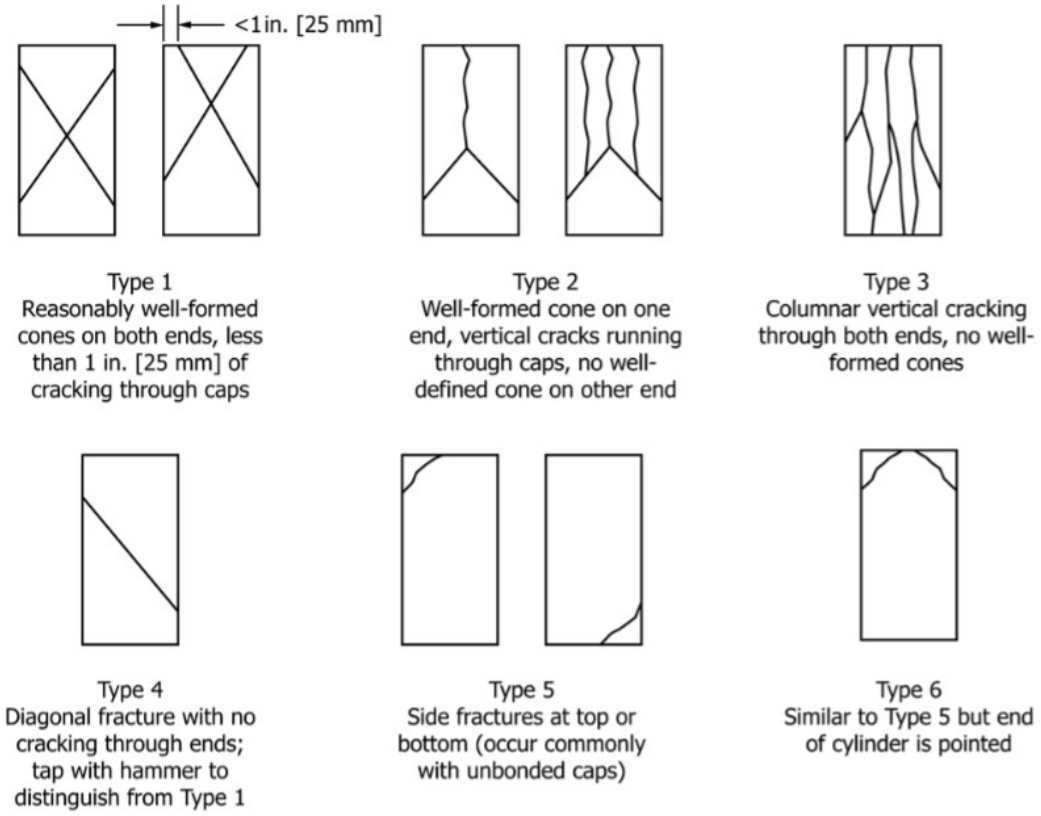

Figure 27: compression test typical fracture patterns from ASTM C39

Figure 28: fracture patterns as observed during testing (Types 3/5/6 and 2)

8.2.3 Thermogravimetric analysis (TGA)

The thermogravimetric analysis was conducted on 4 samples in nitrogen atmosphere at 60ml/min gas flow across the sample. The sample details and analysis results are pictured in Figure 29 for samples of different curing times.

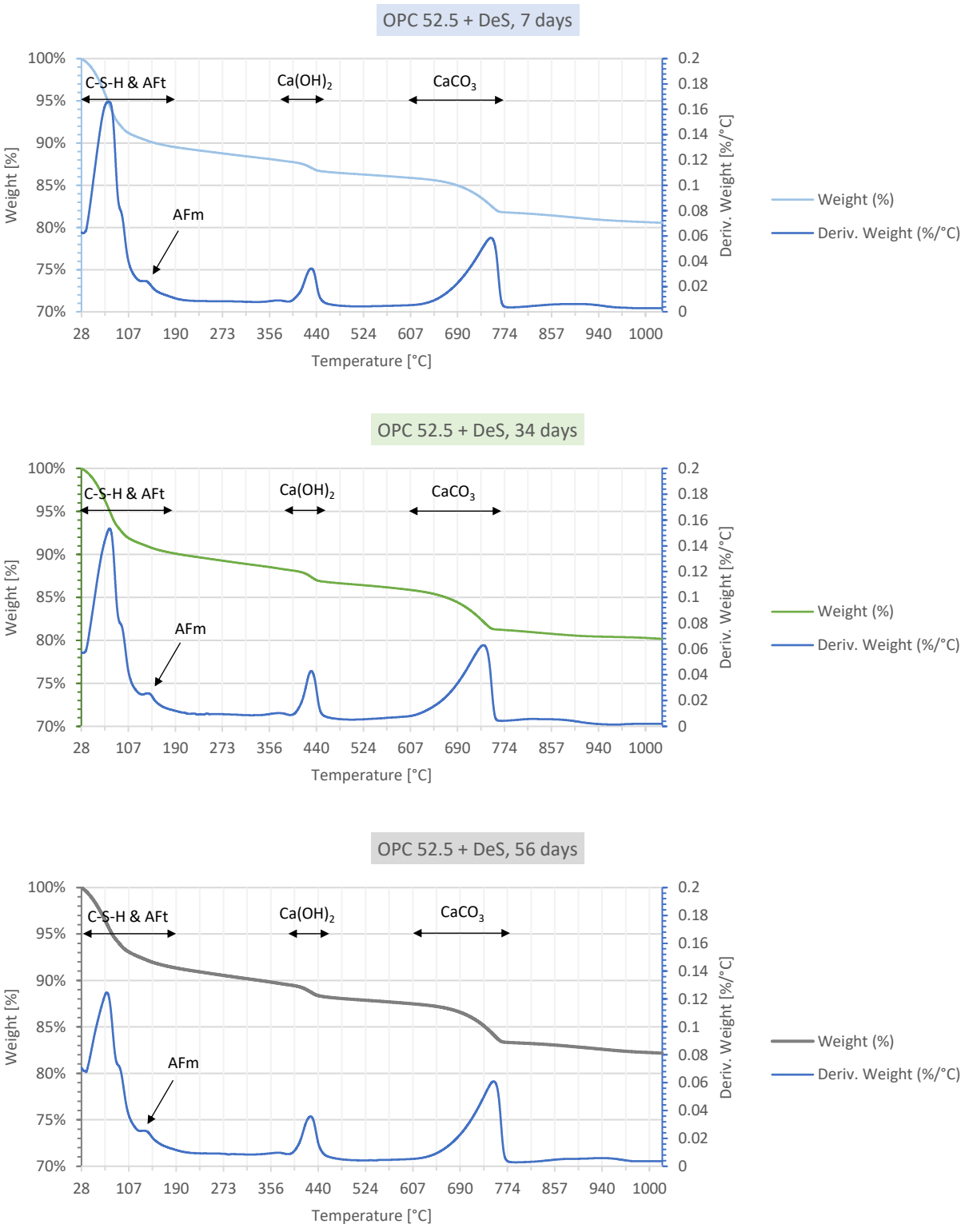

Figure 29: TGA of OPC+DeS samples, 7, 34 and 56 days

Figure 29 shows the degradation of the OPC+De-S samples after 7, 34 and 56 days – exact composition of the samples can be found in chapter 6.2, section (III). Decomposition starts almost immediately at below 40°C, which can be attributed to the mass loss from water evaporation and decomposition of hydrates, such as C-S-H paste and ettringite. (Tantawy, 2017) However, the exact mass loss is difficult to allocate as it is overlapping among several phases. A small peak due to the decomposition of monosulfate (AFm) is further visible at around 150°C. As temperature increases, the decomposition rate achieves 2 more signifiant peaks, which can be attributed to portlandite dehydration at around 400°C which formed during the hydration of cement. Finally, the decarbonation of $CaCO_3$ occurs between 650-750°C. $CaCO_3$ is formed due to the carbonation of the slag aggregate during processing. Around 80% of sample mass remains intact after the heating.

The decomposition mode, as well as the values for onset temperature (IDT) and final residue (FR) do not vary significantly for different curing time. However, while the mass loss attributed to portlandite and calcium carbonate is relatively constant, the rate of decomposition of hydrates (below approximately 150°C) is lower for higher curing times, as can be seen from the initial mass loss in Table 14. This may be due to less free water present after longer curing times, but to make a definite judgement, an XRD analysis would be necessary to evaluate the microstructure and reacted compounds in the material.

The mass loss during decarbonation of $CaCO_3$ finally gives an indication of the sequestered carbon in our material, which will be further discussed in chapter 10.

Additionally, a trend of higher onset temperature, higher final residue and generally higher thermal stability can be seen for long curing time (56 days).

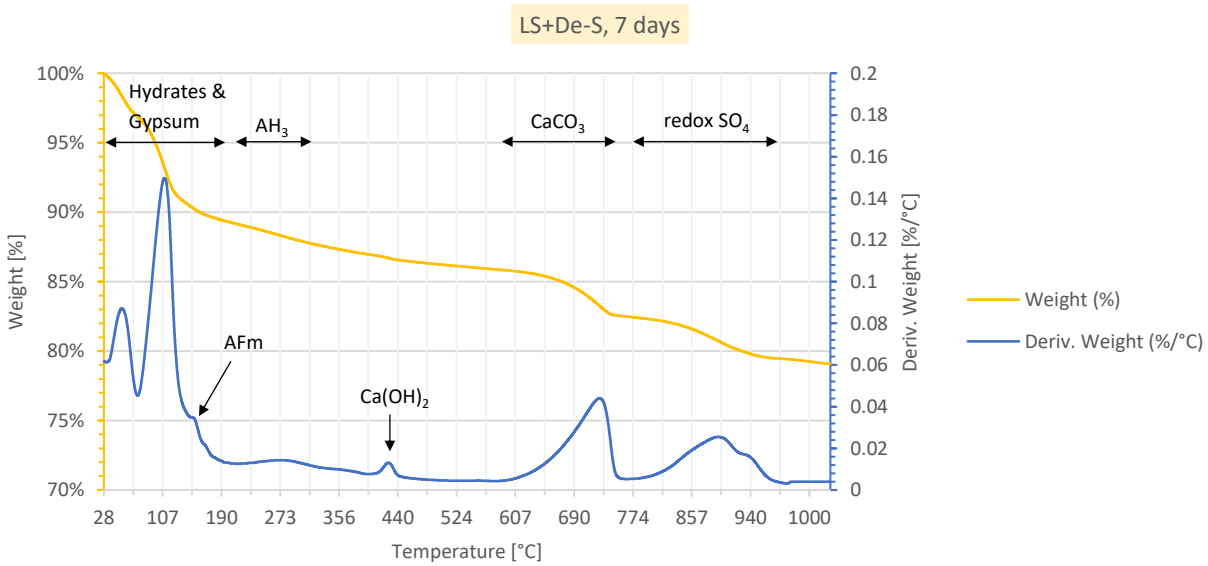

Figure 30: TGA of LS+DeS samples, 7 days

Figure 30 depicts the degradation curve of LS+De-S mix that was researched initially. The exact composition of the samples can be found in chapter 6.2, section (II). This sample degrades at different mode than the OPC-based samples, with immediate degradation onset and a first degradation rate peak at 42°C. Again, this is due to water and hydrates present in the sample, this time predominantely ettringite, with a small peak of monosulfate at 150°C as seen in the OPC-based samples. Smaller quantities of aluminium hydroxide from the reaction between LS and Gypsum also cause a low peak between roughly 200 and 300°C. We can see two initial peaks instead of one – a (usually smaller) second peak at 110-120°C occurs in similar mixes due to unreacted gypsum in the sample which acts as a hydration retarder to control workability, especially for Al-containing phases. However as this peak is quite significant and at slightly higher temperature than expected, it is unlikely to be due to unreacted gypsum only. As we have no cement present in this sample, the quantity of portlandite is very small and hence only a small peak is visible at around 400°C. The decarbonation reaction of $CaCO_3$ evidenced in the graph at around 700°C is slightly lower compared to the cement-based samples, as this mix contains around 10% less of the carbonated De-S slag. Finally, we can also observe a slight mass loss at approximately 900°C, which may be due to the reduction–oxidation reaction of SO_4 (Nguyen, et al., 2021).

Overall, the material exhibits more, but lower peaks in degradation rate and a total relative mass loss slightly higher than for the OPC-based sample.

In terms of thermal stability, the OPC based samples exhibit higher thermal stability with minor variations depending on curing time. Nevertheless, the initial decomposition and maximum decomposition rate temperatures are generally low at <70°C, which could be dangerous depending on the application. (Tiwari, 2015) For OPC, we typically observe higher IDT at around 100°C, and compressive strength is halved at approximately 600°C with almost complete loss of strength above 800°C. (Tantawy, 2017)

Table 14: mass loss of different phases in samples

material	curing [days]	initial ML [%]	Portlandite ML [%]	$CaCO_3$ ML [%]	Redox ML [%]
OPC+DeS	7	10.6	1.2	4.1	-
OPC+DeS	34	10.0	1.4	4.6	-
OPC+DeS	56	8.7	1.3	4.2	-
LS+DeS	7	10.7	<1.0	3.5	3.0

Some values relating to mass loss and thermal stability are summarised in the following Table 15 and Figure 31.

Table 15: thermal stability parameters of sample

material	curing [days]	ini. weight [mg]	FR [mg]	FR [%]	IDT [°C]	MRD [%/°C]	TGA date
OPC+DeS	7	69.895	56.31	80.56%	<65.47	0.1661	28/07/2021
OPC+DeS	34	63.792	51.25	80.34%	<66.46	0.1533	30/08/2021
OPC+DeS	56	79.801	65.69	81.31%	<68.83	0.1246	30/08/2021
LS+DeS	7	54.876	43.39	79.08%	<42.00	0.0872	28/07/2021

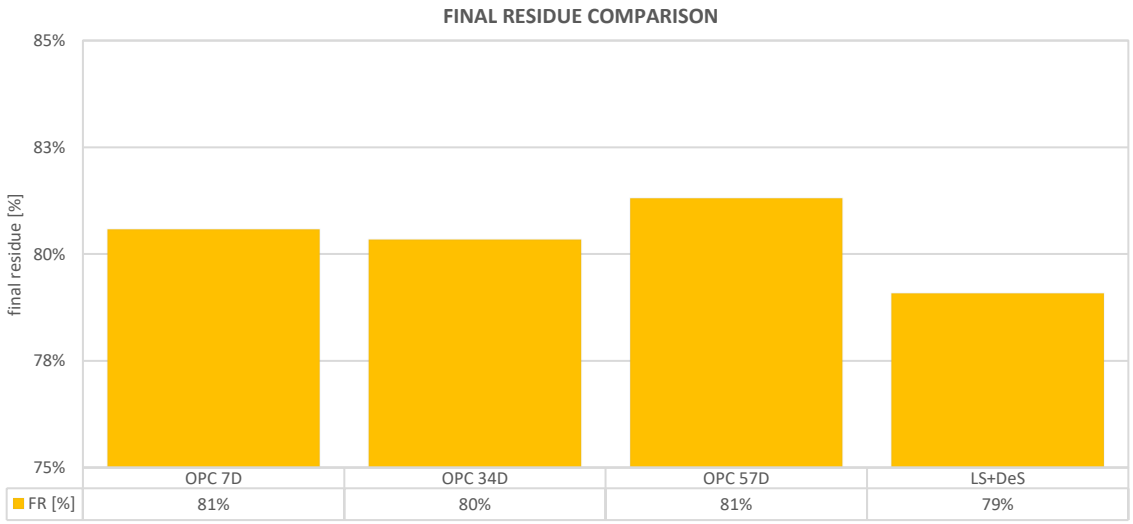

Figure 31: final residue of samples in percent of initial mass

8.2.4 Durability tests

The freeze-thaw test was conducted for 6 samples as outlined in chapter 7.3, with half the samples saturated in water, and the other half saturated using de-icing solution with 3wt% of NaCl. The testing process was 28 days in total, split into the following sections:

Days 0-7: pre-saturation of specimens

Days 7-14: freeze-thaw cycling (14 cycles)

Days 14-21: re-saturation of specimens

Days 21-28: freeze-thaw cycling (14 cycles)

The results that were considered for this analysis are the compressive strength, density changes, scaling resistance and a visual assessment. The sample details are summarised in Table 16 below for reference. It should be noted that the samples have a lower l/d ratio than the ones used for previous tests due to limited material supply. Sample H_2O - 3 in particular has a l/d ratio < 1.

Table 16: OPC52+DeS aging samples details

sample	description	solution	casted	start test	end test	days cured
NC-1	OPC52+DeS	NaCl	06/09	12/10	09/11	36
NC-2	OPC52+DeS	NaCl	06/09	12/10	09/11	36
NC-3	OPC52+DeS	NaCl	06/09	12/10	09/11	36
W-1	OPC52+DeS	water	07/09	12/10	09/11	35
W-2	OPC52+DeS	water	07/09	12/10	09/11	35
W-3	OPC52+DeS	water	07/09	12/10	09/11	35

Density changes

The samples were weighted and measured before and after each pre-saturation and freeze-thaw cycling. The results for the mass changes in wt% are summarised in Table 17.

Table 17: OPC52+DeS aging samples mass changes

sample	Day 7 [%]	Day 14 [%]	Day 21 [%]	Day 28 [%]
NC-1	2.41	-1.14	3.24	-0.9
NC-2	3.62	-0.35	4.22	-0.08
NC-3	2.9	-0.76	3.52	-0.56
W-1	2.93	-0.64	3.87	-0.91
W-2	2.53	-0.44	4.23	-0.75
W-3	1.66	-1.23	2.69	-1.31

As evidenced from Figure 32 and Figure 33, the uptake of saturation liquid increases significantly after the first set of freeze-thaw cycles (day 21) compared to the uptake pre-cycling. While the initial liquid uptake during pre-saturation (day 7) is similar for all samples, the increase of uptake after the re-saturation (day 21) is slightly higher for the specimens submerged in water only, with up to 40% higher uptake compared to pre-saturation. Overall, the liquid uptake varies in between 1.7 – 4.2%.

The mass loss occurs after each freeze-thaw cycle and varies in between 0.1 – 1.3 % compared to the initial state. It should be noted that for de-icing solution samples, the mass loss is higher after the first set of freeze-thaw cycles (day 14) compared to the final mass loss. Overall, water-soaked samples had higher mass losses compared to de-icing solution samples.

While Eurocodes do not provide any limitations on mass loss, the GB/T 50082 Chinese standard specifies a mass loss limit of 5%, at which complete damage of the sample can be assumed, which is not reached in this case after 28 cycles. (Zhang, et al., 2014)

The density of the material after curing is 2.16 g/cm^3 on average, which is within the range of a normal density concrete. This reduces to 2.14 g/cm^3 on average post-cycling. The density was evaluated with the formula:

$$\rho\ [g/cm^3] = \frac{m}{V}$$

Overall, the volume of the specimens pre- and post-experiment do not vary to the precision of 1mm. It is concluded that no shrinkage or expansion occurs and density changes correlate with mass changes only.

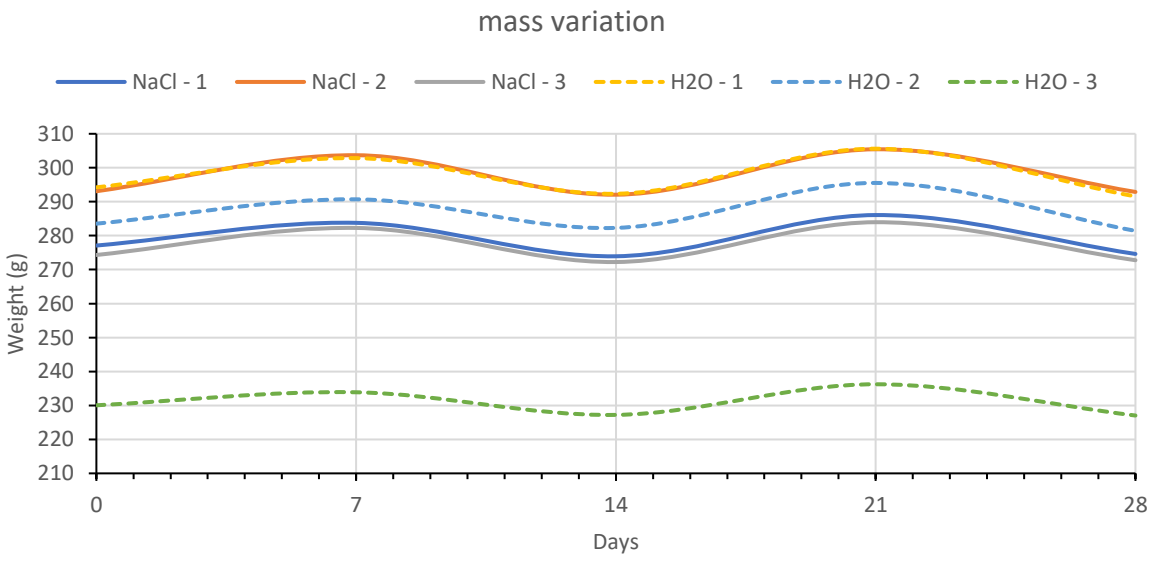

Figure 32: OPC+DeS: mass variations during freeze-thaw cycling

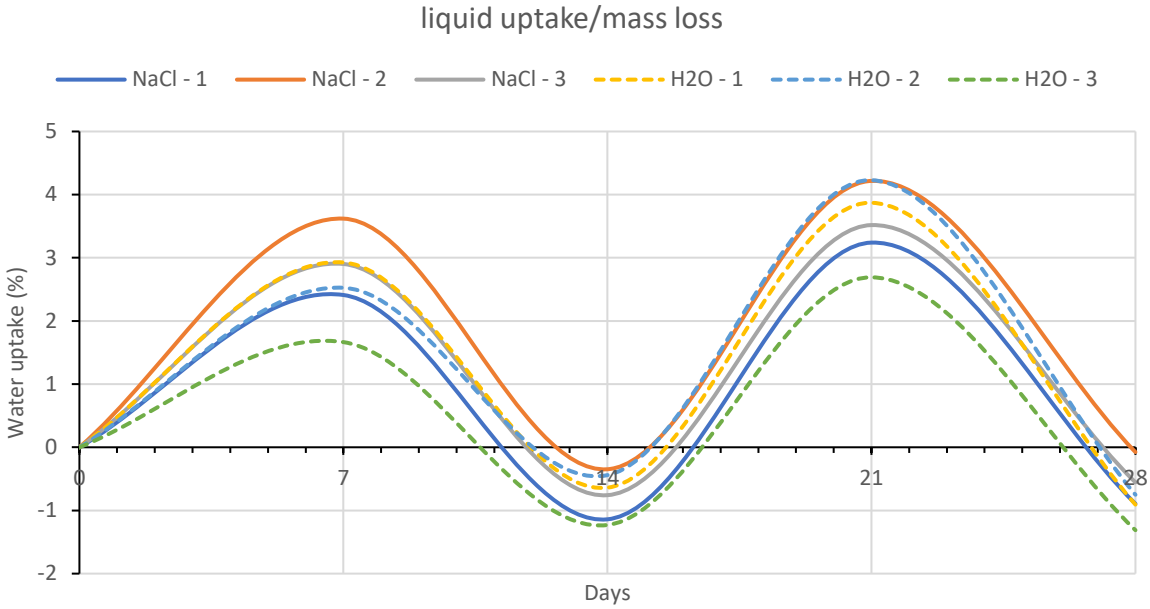

Figure 33: OPC+DeS: liquid uptake during freeze-thaw cycling

Other factors affecting the freeze-thaw resistance are porosity and permeability. Higher permeability of materials is sometimes viewed as beneficial in terms of freeze-thaw resistance of concrete, as it may allow hydraulic pressures in the material structure to dissipate more readily and in turn prevents microcracking. (Bogas, et al., 2016) On the other hand, high permeability may be a disadvantage as it allows a quicker and easier saturation of the material. BS 8007 recommends low permeability for higher leaching, erosion, abrasion and freezing-thawing resistance. The standards further provide aggregate size and water absorption limits for freeze-thaw resistance. The limit on water absorption of aggregates is generally retained at 2-3% maximum in critical conditions such as aggressive freeze-thaw exposure. However, the CIRIA Report C559 suggests, that in light of the high freeze-thaw resistance of lightweight concrete which often employs aggregates of higher water absorption, such limits may not always be meaningful. (The Concrete Society, 2014)

Visual assessment and scaling resistance

The specimens before and after the experiment do not show any severe damage such as cracks, pop-outs or scaling and look relatively undamaged to the naked eye. The results suggest a very good scaling resistance of the material, fulfilling the requirements given in EN 13877 for concrete pavements of category FT0 and FT1. For further classification of the material, the scaling after 56 cycles must be evaluated.

Pictured in Figure 34 and Table 18 are the specimens at the beginning of the testing procedure and after. Changes in colour are mainly due to lighting and saturation differences but do not indicate any damage.

Figure 34: specimens pre aging

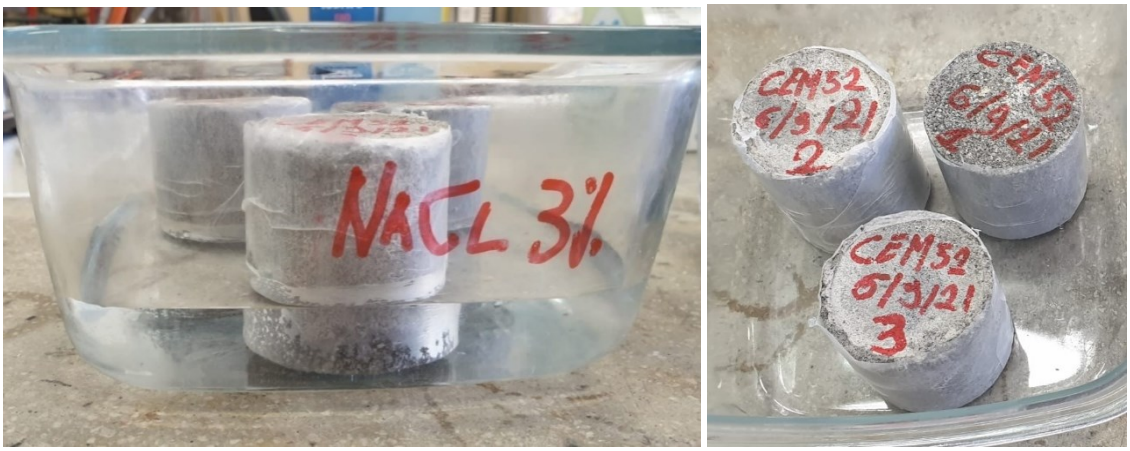

Table 18: specimens post aging

	top	bottom
NaCl – 1	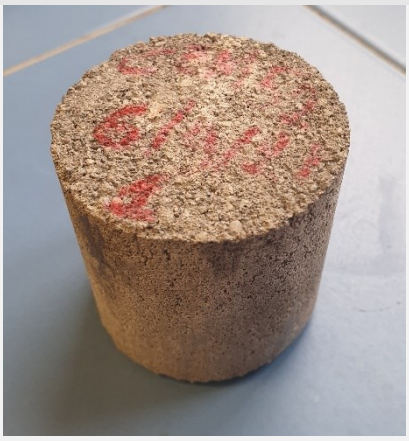	
H2O – 1	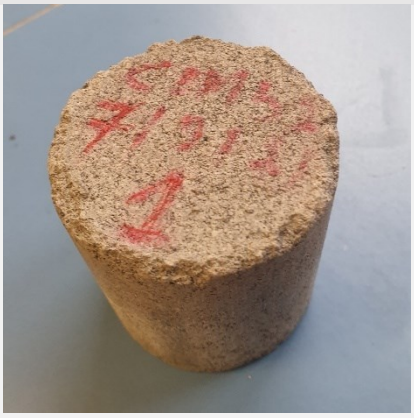	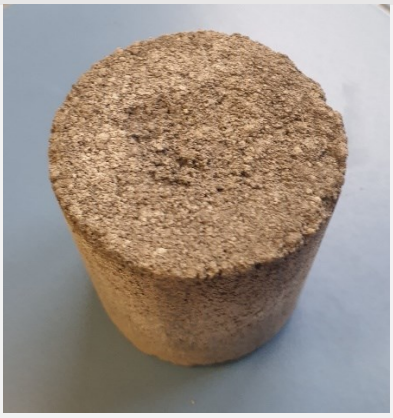

Residual compressive strength

To evaluate the strength of the samples post-experiment, the specimens were tested in compression one week after conclusion of the freezing-thawing cycles. As before, conversion factors (CF) provided in the technical standard ASTM C42 were used to compare strength.

$$f_{ck,cyl,corr} = f_{ck,cyl} * CF$$

It is not recommended to test specimens of l/d < 1.0 as results may not be representative. Hence, the results for sample W-3 were not taken into consideration.

Results for the compressive strength and modulus of elasticity are collected in Table 19.

Table 19: OPC52+DeS: aging residual compressive strength

sample	description	solution	casted	cured	l/d	max. load P	compr. strength f_{ck}	CF	corr. $f_{ck,cyl}$	Young's mod
				[days]	[-]	[kN]	[MPa]	[-]	[MPa]	[GPa]
NC-1	OPC52+DeS	NaCl	06/09	36	1.0	27.92	12.06	0.87	10.49	0.89
NC-2	OPC52+DeS	NaCl	06/09	36	1.1	33.93	14.65	0.89	13.10	1.05
NC-3	OPC52+DeS	NaCl	06/09	36	1.0	38.25	16.46	0.87	14.32	1.05
W-1	OPC52+DeS	water	07/09	35	1.1	26.52	11.45	0.89	10.24	0.82
W-2	OPC52+DeS	water	07/09	35	1.1	25.37	10.91	0.89	9.76	0.84

The results of previous experiments for comparable curing time (31-34 days) show, that the effect of freezing-thawing cycles is negligible and seem to have no effect on compressive strength. Considering also the fact that no volume changes occurred during the experiment, we can assume that the material was able to accommodate expansion of capillary liquid. Hence, no microcracking and damage was apparent after 28 cycles.

However, the slightly lower values of elastic modulus indicate a lower stiffness of the samples after aging. To verify this relationship, more tests are necessary.

no freeze-thaw cycling		post 28 freeze-thaw cycles	
$f_{ck,1}$ [MPa]	E [GPa]	$f_{ck,2}$ [MPa]	E [GPa]
11.15	1.40	11.58	0.93

The stress-strain diagrams for the specimens subjected to aging (Figure 35 and Figure 36) do not show significant variations in behaviour compared to previous experiments. In fact, the samples saturated in 3wt% NaCl solution show better results than water-saturated samples.

While the small number of test specimens cannot give precise results, the experiment showed promising results and indicated a very good freeze-thaw resistance of the material.

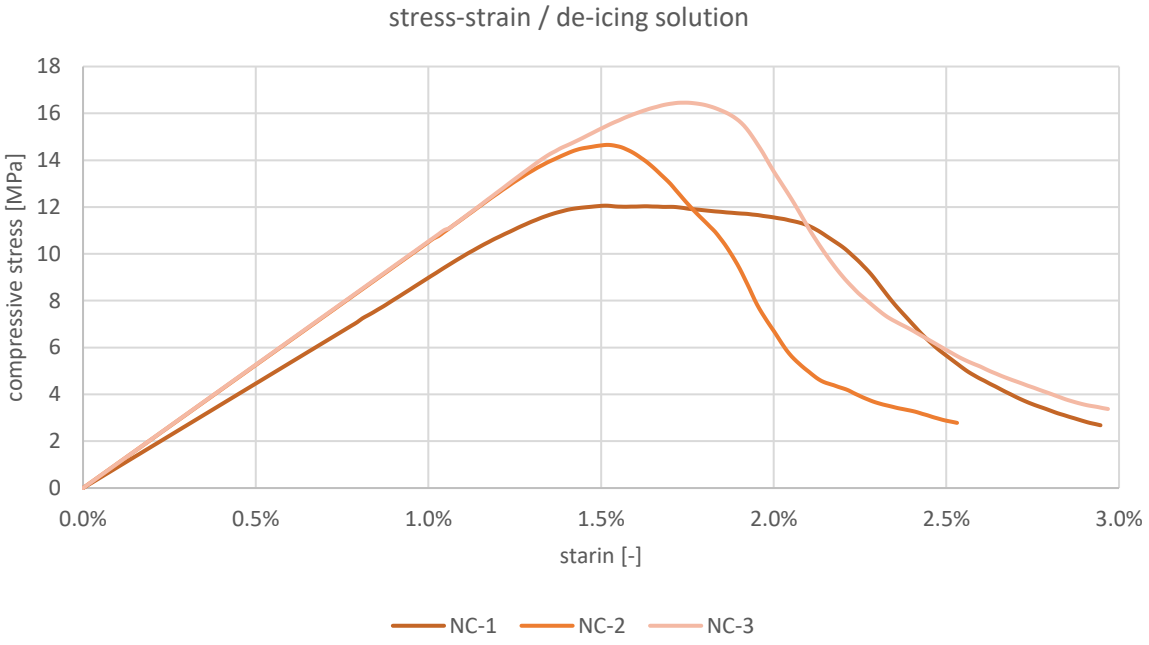

Figure 35: OPC52+DeS NaCl+water saturated: compressive strength after aging

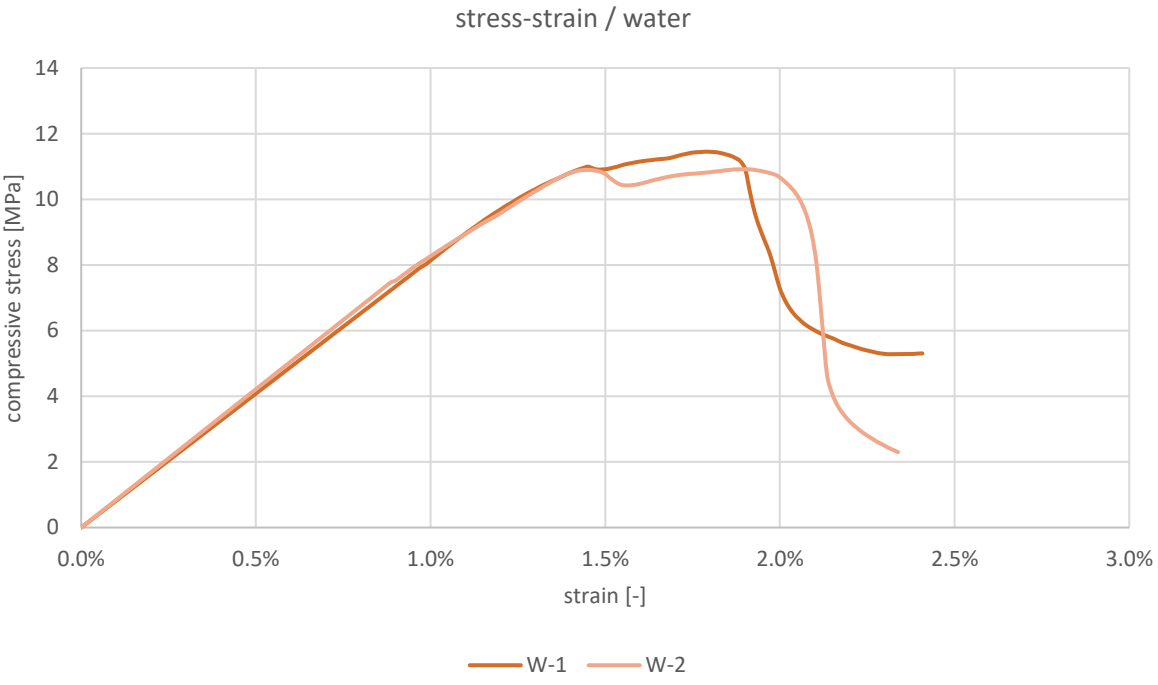

Figure 36: OPC52+DeS water saturated: compressive strength after aging

9. Comparison and Classification

The EN 206:2013 specifies the classes for compressive strength of concrete. The characteristic compressive strength considered in the standard refers to 300mm cylinders with l/d = 2, or 150mm cubes cured for 28 days before testing.

L/d ratio

For the specimens with an l/d ratio of ≤1.75, the maximum compressive strength was previously multiplied by a correction factor, which was interpolated from the values given in ASTM C42.

Dimensions

The ASTM as well as the Eurocode recommends a height of 200-300mm for test cylinders, while the specimens used in this research are just below 100mm. Some research such as by (Sudin & Ramli, 2014) suggests that with similar l/d ratio, compressive strength varies only slightly with specimen dimensions, with the general consensus being that compressive strength increases slightly with cylinder dimension decrease. Several research papers however suggest that such differences are significant, and many such as (Hossen, et al., 2015) developed parameters for calculating the compressive strength for varying cylinder dimensions. To compare the compressive strength of 50mm cylinder diameter to a 150mm diameter standard specimen, a conversion factor of 1.6 is recommended:

$$f_{ck,cyl\emptyset=150mm} = f_{ck,cyl\emptyset=50mm}/1.6$$

Research by (Gyurkó & Nemes, 2020) further suggests that lower-strength concrete is more affected by strength variations due to size compared to higher strength concrete, as lower strength concrete is associated with a higher level of inhomogeneity. In fact, research on higher strength concrete by (Tokyay & Özdemir, 1997) using smaller cylinders of 50mm diameter compared to larger specimen sizes of 100-150 mm diameter, claims that smaller specimens may give results of significantly lower apparent strength in comparison to larger standard specimens, due to the so-called “wall-effect”.

The conversion factor mentioned here will be considered in the calculation, but the result should be treated with caution, as no official guidelines have been established for specimen dimension comparison and conversion.

As concrete is classified with both cylindrical and associated cube strength, the latter was calculated using a correction coefficient. The EN 206-1 among others uses a coefficient of approximately 0.8 for comparison of cube and cylindric strength.

$$f_{ck,cyl} = f_{ck,cube} \times 0.8$$

The l/d ratios, correction factors for l/d ratio and final corrected cylindric and cube strengths for 50 and 150mm diameter cylinders of the cement-based samples (OPC52.5+DeS) are collected in Table 20 below.

Table 20: OPC+DeS: corrected/converted values for compressive strength

					Ø=50mm		Ø=150mm	
sample	cured	c. strength fck	l/d	CF	corr. $f_{ck,cyl}$	$f_{ck,cube}$	corr. $f_{ck,cyl}$	$f_{ck,cube}$
	[days]	[MPa]	[-]	[-]	[MPa]	[MPa]	[MPa]	[MPa]
S09	27	8.21	1.72	0.98	8.03	10.04	5.02	6.27
S10	27	10.32	1.72	0.98	10.09	12.61	6.31	7.88
S11	27	13.33	1.72	0.98	13.03	16.29	8.15	10.18
S12	18	9.80	1.72	0.98	9.58	11.97	5.99	7.48
S13	18	9.12	1.72	0.98	8.91	11.14	5.57	6.96
S14	18	12.40	1.72	0.98	12.13	15.16	7.58	9.47
S15	56	11.24	1.76	1.00	11.24	14.05	7.03	8.78
S16	56	14.22	1.85	1.00	14.22	17.77	8.89	11.11
S17	56	11.62	1.76	1.00	11.62	14.53	7.27	9.08
S21	7	6.76	1.72	0.98	6.61	8.26	4.13	5.16
S22	7	6.80	1.72	0.98	6.65	8.31	4.16	5.19
S23	7	4.73	1.72	0.98	4.62	5.78	2.89	3.61
S24	34	12.03	1.59	0.97	11.64	14.54	7.27	9.09
S25	34	10.73	1.78	1.00	10.73	13.41	6.70	8.38
S26	34	9.47	1.64	0.97	9.20	11.50	5.75	7.19
S27	31	11.95	1.59	0.97	11.56	14.45	7.22	9.03
S28	31	13.02	1.62	0.97	12.62	15.78	7.89	9.86

The results for durability analysis were normalised for l/d ratios previously. The results and corresponding cube strength are collected in Table 21 below.

Table 21: OPC+DeS post aging: corrected/converted values for compressive strength

							Ø=50mm	
sample	description	solution	cured	l/d	compr. strength f_{ck}	CF	corr. $f_{ck,cyl}$	corr. $f_{ck,cube}$
			[days]	[-]	[MPa]	[-]	[MPa]	[MPa]
NC-1	OPC52+DeS	NaCl	36	1.0	12.06	0.87	10.49	13.11
NC-2	OPC52+DeS	NaCl	36	1.1	14.65	0.89	13.10	16.38
NC-3	OPC52+DeS	NaCl	36	1.0	16.46	0.87	14.32	17.90
W-1	OPC52+DeS	water	35	1.1	11.45	0.89	10.24	12.80
W-2	OPC52+DeS	water	35	1.1	10.91	0.89	9.76	12.20

Comparison to concrete

As evidenced in Table 20, the characteristic compressive strength of the specimens after 27 days of curing ranges between 8/10 and 13/16 MPa for cylinder/cube, when the correction factor for specimen dimensions is not considered. This would correspond to the lowest possible compressive strength class of concrete, C8/10. However, for longer curing time of 56 days, the composite reaches a compressive strength of possibly up to C12/15.

The composite could be classified as very weak normal-grade concrete, which is suitable for non-structural application. The use of the material is limited to filling and slab for garages, patios, pathways and low-load domestic floors and foundations. As shown in the freeze-thaw experiment results in chapter 8.2.4, the composite scaling resistance fulfils the requirements of EN 13877 for concrete pavements of category FT0 and FT1.

Taking into account the conversion factor for dimensions by (Hossen, et al., 2015), the composite is below the limits for normal-grade concrete classification. Comparison to concrete in this case is not likely.

Comparison to mortar

EN 998-2 Section 5.4 gives specifications for compressive strength of mortars for masonry. Test specimens for masonry are specified in EN 1015-11 as 40mm test cubes after 28 days of curing, which should be approximately comparable to the corrected compressive cube strength corresponding to $f_{ck,cyl}$ with diameter of 50mm.

The $f_{ck,cube}$ (Ø=50mm) at 27 days of curing ranges between 10 and 16 MPa. This is comparable to average mortar and would most closely correspond to mortar classes M10 and M15. As mortar is used not just to withstand compressive forces, but also to bind, fill and seal bricks, the compressive strength parameter is only an isolated indicator of the composite's suitability as mortar. Further tests are needed to determine other parameters such as bond strength, thermal conductivity and flow tests, as well as an in-depth analysis of water absorption and permeability.

An important aspect for mortars is durability. The composite performed very well in preliminary aging tests, showing no scaling or compressive strength loss after 28 freezing-thawing cycles. The material also exhibited acceptable water absorption and no significant shrinkage or expansion in this timeframe. While more data is needed to verify the materials performance after aging, the initial results indicate suitability for use as mortar also in more aggressive environments.

10. Environmental Impact

A life cycle assessment of the composite was attempted to evaluate the environmental impact. The parameter considered for impact assessment was the embodied carbon of the material for the product stage only. The analysis is conducted using a modified version of the ICE Cement, Mortar and Concrete Model which was sourced from the ICE website.

The functional unit of the material was identified as 1 kg.

The EN 15978 specifies several stages for consideration in a life cycle assessment, pictured in Figure 37. The product stage A1-A3 was identified as relevant for this analysis, which comprises the raw material supply, transport, and manufacturing. Some considerations of the end-of-life stage were attempted also.

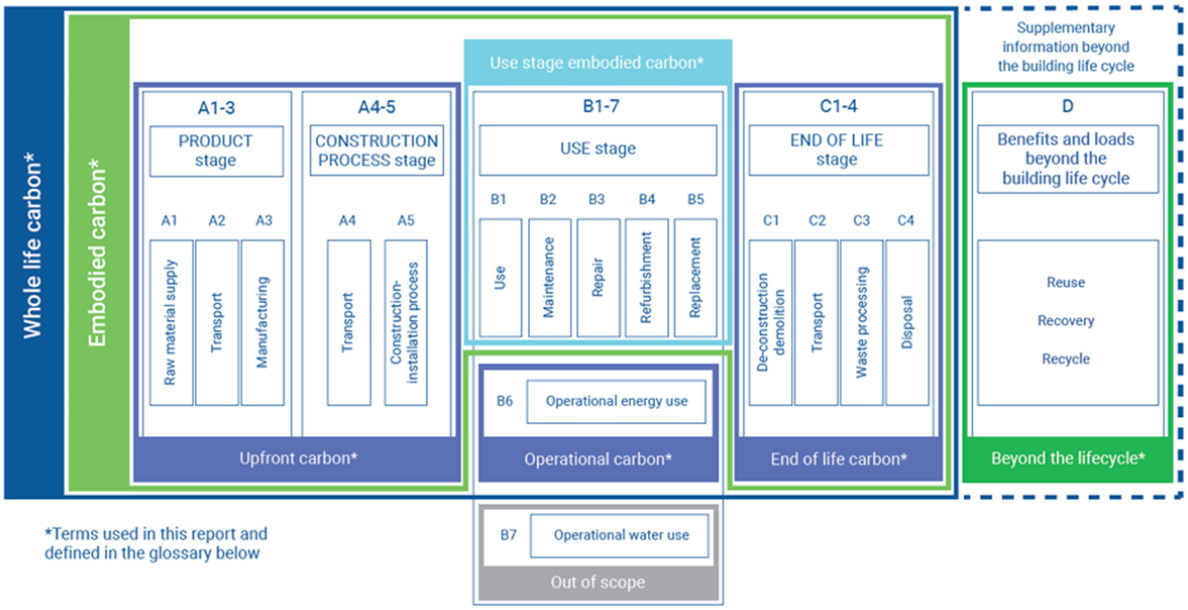

Figure 37: LCA stages

The materials considered for comparison are the mixes considered throughout this paper. Ladle Slag based mixes LS+BOF, LS+DeS

- Cement and Ladle Slag based mix OPC+LS+DeS
- Cement-based mixes OPC+DeS.

The exact constitution of each is specified in previous chapters.

The embodied carbon for each mix is estimated based on available data and compared to that of the average European CEM I.

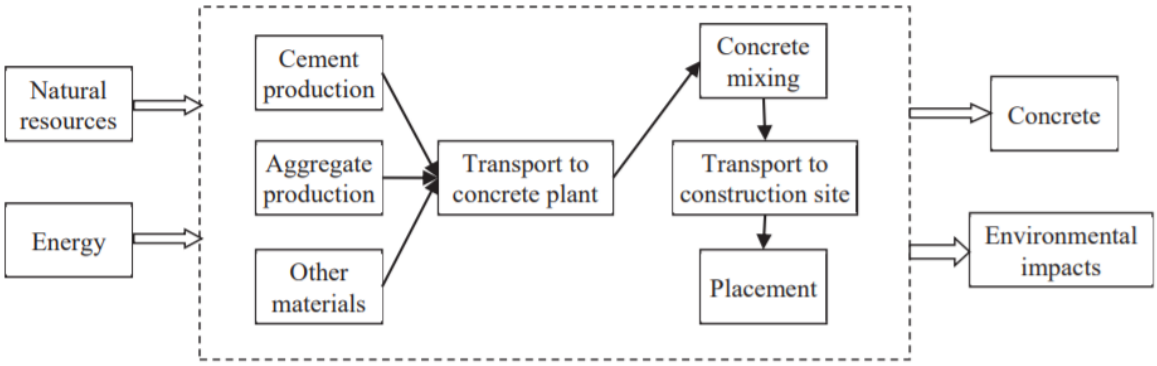

Figure 38: System boundary for concrete production (Anastasiou, et al., 2017)

10.1 Embodied carbon estimation of components

To estimate the embodied carbon of the composites used in this research, the emissions corresponding to each material component are evaluated.

Embodied Carbon of cement

The embodied carbon of European CEM I is estimated at 898 kgCO2e/tonne (Cembureau, 2015) for the product stage A1-A3.

Embodied Carbon of sand

For the reference mortar mix, sand was used as aggregate. Research by (Ma, et al., 2016) estimates the sand production for use in a concrete/mortar mix to produce 5.36 kgCO2e/tonne, which is mainly due to the electricity consumption during processing and transportation.

Embodied Carbon of Ladle Slag

Processes that were not considered for embodied carbon calculations of ladle slag are the following:

- Alteration of landscape – while steel manufacturing plants do have an impact on landscape and society, these impacts do not translate to recycled by-products of steel manufacture such as ladle slag.
- Materials extraction – the ladle slag was received from the factory, after being naturally cooled and collected at a slag cooling pit. The energy required for such a process is negligible.

Processes that were considered for embodied carbon calculations of ladle slag are the following:

- Freight Transport

Trucking was considered for the material transport to the production site. As steel plants are available across Europe, the maximum trucking distance was assumed to be 500km. The ICE

LCA tool provides a value of 0.00499 kgCO_2e/kg per 30 miles both ways, based on values by (Defra, 2018).

From this, the impact of 500km trucking is calculated as 0.0499 kgCO2e/kg.

- Aggregate processing

The material requires sieving and milling before use. Sieving is not considered in the calculation as it was done by hand. The impact of milling was evaluated based on energy needs of machinery, milling time and local electricity emissions.

Time required for milling t = 20x2 minutes for 1kg of slag = 0.67 h

Power of machine *FRITSCH planetary mill pulverisette 5* P = 2.2 kW

Electricity emissions (Italy) e = 0.2134 kgCO2e/kWh (European Environment Agency, 2021)

$$P[kW] * t[h] * e[kgCO_2e/kg] = 0.313\ kgCO_2e/kg$$

The impact of milling is estimated at 0.313 kgCO2 per kg milled slag. Only 65-80% ladle slag was used in milled form, so the values are recalculated for each mix to take this into account.

- Mixing and preparation

Material batching and casting accounts for the mixing and preparation emissions. The values from the ICE cement, mortar and concrete model database (Inventory of Carbon and Energy (ICE), 2019) were used for this, using European or UK average data.

Embodied carbon of BOF/De-S slag

The aggregate slags do not require any additional processing. Both materials were carbonated in the laboratory, with TGA results in chapter 8.2.3 indicating a CO_2 content of approximately 5%. Hence the final sequestered amount of CO_2 is estimated at 50 gCO_2/kg. Transport was calculated the same as for ladle slag.

The final embodied carbon of aggregate slags is the sum of carbon sequestered during preparation and the transport which amounts to the almost net-zero value of -0.087 kgCO_2/ton.

Embodied carbon of other materials

The embodied carbon values of other materials used in the process were provided by the ICE database (Inventory of Carbon and Energy (ICE), 2019) for the following:

Gypsum = 0.002536 kgCO_2/kg
Water = 0.000344 kgCO_2/kg
Citric Acid = 0.41 kgCO_2/kg
Hydrated Lime = 0.891 kgCO_2/kg

10.2 Comparison

The final embodied carbon is calculated based on the composite composition by wt%. The reference concrete is evaluated using a composition of 3:1:12 of cement, lime and sand. Water is assumed to make up 40wt% of the mix.

The findings are summarised in Figure 39. It is evident from the values, that a significant reduction was achieved using recycled and carbonated steel slags. The initial mixes were able to achieve a reduction of emissions of up to 75% compared to the reference mortar, and the final OPC-based composite still achieved a reduction of approximately 40% despite re-introducing cement.

The graph also highlights the biggest sources of emission, which unsurprisingly is cement. Ladle slag also has a significant impact, which could however also be down to the rather energy-intensive processing in the lab compared to mass production. Overall, the carbon savings achieved in the material are less due to the employment of sustainable aggregate, but rather the reduction and replacement of cement with more aggregate or ladle slag. It is evident, that the aggregate is only responsible for a very small fraction of emissions and the impact of sustainable alternatives on this front is low.

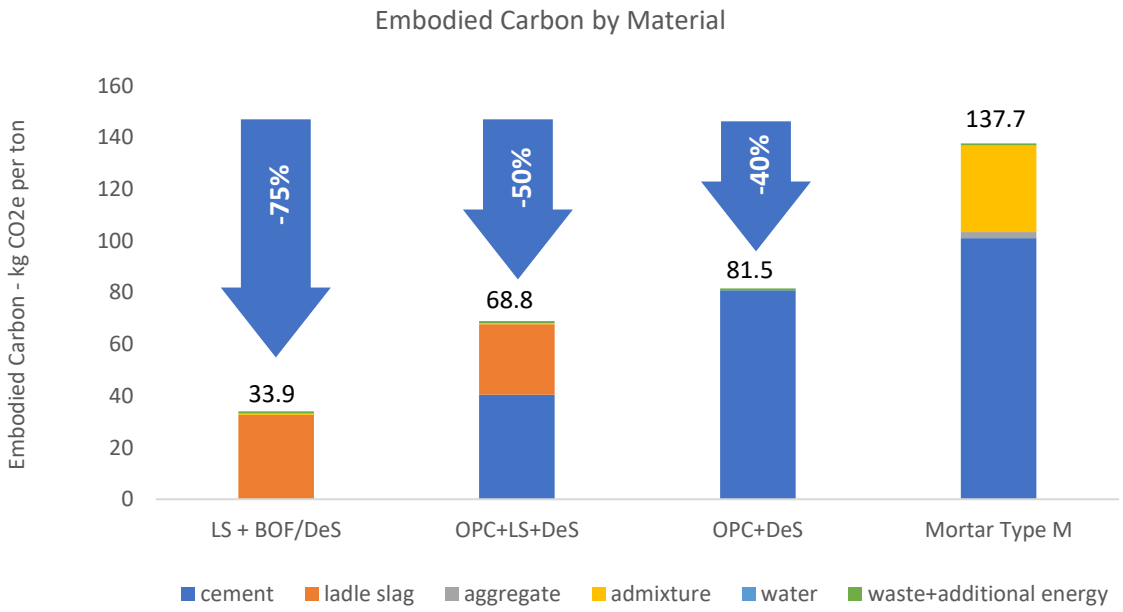

Figure 39: embodied carbon of materials researched compared to conventional mortar

End of life considerations

Since the materials used in this mix can be toxic for aquatic life and the environment in general (Terrones-Saeta, et al., 2021), they need to be safely disposed of. Recycling is possible by crushing and re-using the material as filler. End-of-life release of sequestered carbon is very unlikely unless the material is subjected to high temperatures. In fact, the carbonates in the material such as $CaCO_3$ are very durable and likely to stay trapped for thousands of years.

11. Conclusions

This experimental investigation studied the compressive strength, stress-strain behaviour, and other properties of two distinct composites, namely ladle-slag based composites (LS+BOF and LS+De-S) and cement-based composites (CEM+De-S).

- First tests of ladle-slag based materials indicate a weak performance of the composite. There is a significant difference also in strength between the composites employing BOF and De-S slags, with the latter showing approximately 20-30% lower compressive strength. Overall, the LS-based samples did not exceed 3 MPa in compressive strength and the experiments were discontinued for the mix.
- In further experiments, a composite of CEM I (52.5MPa) and De-S slag was used. The results were more promising in this case, with compressive strength of up to 13-14 MPa.
- Comparison of compressive strength for different curing times showed increased hydration and consequently higher compressive strength with longer curing time. However, the 7-day strength of the material was relatively low, reaching only 57% of the 27-day strength, while strength gain between 1 and 3 weeks was significant.
- Analysis of stress-strain diagrams of the samples show relatively high deformations before failure as well as a high post-peak energy compared to concrete and some mortars. Higher stiffness may be desirable depending on the application.
- Ageing tests were conducted on some samples via freeze-thaw cycling. The specimens show no scaling or loss of strength after 28 cycles, which indicated a very good frost resistance of the material. Water absorption was acceptable, and no expansion or shrinkage was reported.
- It was possible to reduce the equivalent CO_2 emissions of the material compared to conventional mortar by using recycled aggregates and carbonation of the materials. Initial estimates suggest a reduction of 40% for the best-performing cement-based mix when compared to type M mortar.

The initial findings summarised in this thesis project suggest that the OPC-based composite material could be considered for use as mortar as specified in EN 998-2. However, further research is necessary to investigate material properties and possibly improve the performance.

11.1 Suggested further research

The results of this experimental investigation raise some questions that may require more research.

Optimising material composition

The composites analysed in the scope of this thesis show some promise as a mortar, however more experiments are necessary to evaluate how changes to the material composition could be beneficial to its mechanical performance. An interesting point to further investigate is the quality difference between mixes using the BOF vs. the De-S slag. As the chemical composition of the slags is comparable, the differences in performance could be due to differences in water content. However, the microstructure of the materials could also play a role. De-S slag has more amorphous content than BOF slag, which is largely crystalline. This results in differences of reactivity between the slags.

Further tests for classification

Further tests would need to be conducted to assess the suitability of the material produced during this thesis project for non-structural application or mortar. For the latter in particular, the workable life, water/vapour permeability, water absorption, adhesion and thermal conductivity could be further analysed and quantified, depending on the exact application. (MPA mortar, 2020)

Early strength development

The composite currently exhibits relatively low early strength gain, with only 57% of the 27-day strength reached after 7 days. This is problematic in real-life applications where early strength gain is essential. Further research would be needed to explore how to accelerate the hydration reaction and develop strength faster.

Water content

Several studies have shown that a high moisture content has a negative effect on the compressive strength of concrete (Chen, et al., 2012) as well as mortar (Sugrañez, et al., 2013). This work found that compressive strength in concrete decreases almost linearly with the degree of saturation, and dips at around 90% until recovering some strength in the higher saturation range (Figure 40).

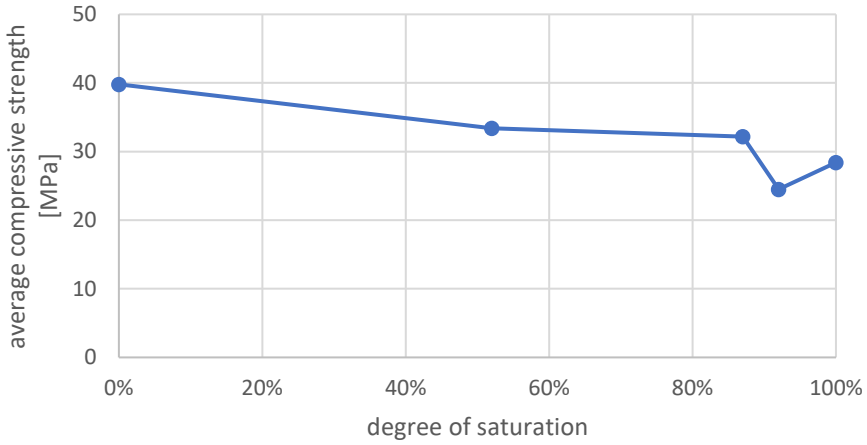

Figure 40: compressive strength of concrete and degree of saturation

This could be of special interest for further research on this project in particular, as the detrimental effect of higher humidity was observed directly in this project. When the BOF slag was replaced with De-S slag in the LS-based recipe, the resulting specimens were for the most part easily crushed by hand, and the few samples that retained some strength performed significantly worse during compression tests. On average, a 20% average reduction of compressive strength was observed when using De-S in the same configuration compared to BOF slag, even with double curing time. Since the chemical composition as well as the PSD does not vary significantly between the two aggregates, there is grounds to assume that the water content could be one reason for the reduced strength, as humidity was higher in the De-S slag. Furthermore, curing in a high-humidity atmosphere caused drastic expansion of the specimens and rendered them useless. It would be interesting to experimentally verify this correlation by varying the water content in the material mix, and/or fully drying the De-S slag before mixing. This could be a way to maximise the compressive strength of the material.

Particle size of raw materials

Research on mortars by (Sugrañez, et al., 2013) shows, that particle size distribution curves are not in direct correlation to compressive strength. However, they are a strong indication that the pore size in the material is directly correlated to mechanical strength. As previously mentioned in chapter 6.1, aggregates of large particle size, especially poorly-graded, result in the formation of large capillary pores that have a detrimental effect on the materials mechanical performance. Literature suggests, that reducing the particle size of cement further results in a higher hydration reaction and increased early strength (Byun, et al., 2010) (Bentz, et al., 1999). However, a smaller-grained mix requires more water, which could outweigh the positive effect. Hence, instead of simply reducing particle size, an optimisation of the PSD would be the best approach to improve mechanical strength (Frigione & Marra, 1976). This would mean both smaller PS and a better graded particle range.

ANNEX

A.1 Particle Size Distribution of Ladle Slag

	PSD from 15/04/21			PSD from 21/04/21			PSD from 09/06/21			PSD from 11/06/21		
PSD [µm]	NET WT [g]	%	CUM.%	NET WT [g]	%	CUM.%	NET WT [g]	%	CUM.%	NET WT [g]	%	CUM.%
<63	664.5	67.98	67.98	711.8	71.84	71.84	662.2	67.05	67.05	412.1	69.10	69.10
63<x<106	77.57	7.94	75.91	71.2	7.19	79.02	76.98	7.79	74.84	42.94	7.20	76.30
106<x<125	27.2	2.78	78.70	36.42	3.68	82.70	46.72	4.73	79.58	29.26	4.91	81.21
125<x<250	124.0	12.69	91.39	113.9	11.49	94.19	121.1	12.26	91.83	72.39	12.14	93.35
250<x<500	40.88	4.18	95.57	32.21	3.25	97.44	39.14	3.96	95.79	24.5	4.11	97.45
>500	43.31	4.43	100.0	25.38	2.56	100.0	41.53	4.21	100.0	15.18	2.55	100.0
Total	1095.0	100.0		990.87	100.0		987.62	100.0		596.37	100.0	

A.2 Stress-Displacement Diagrams

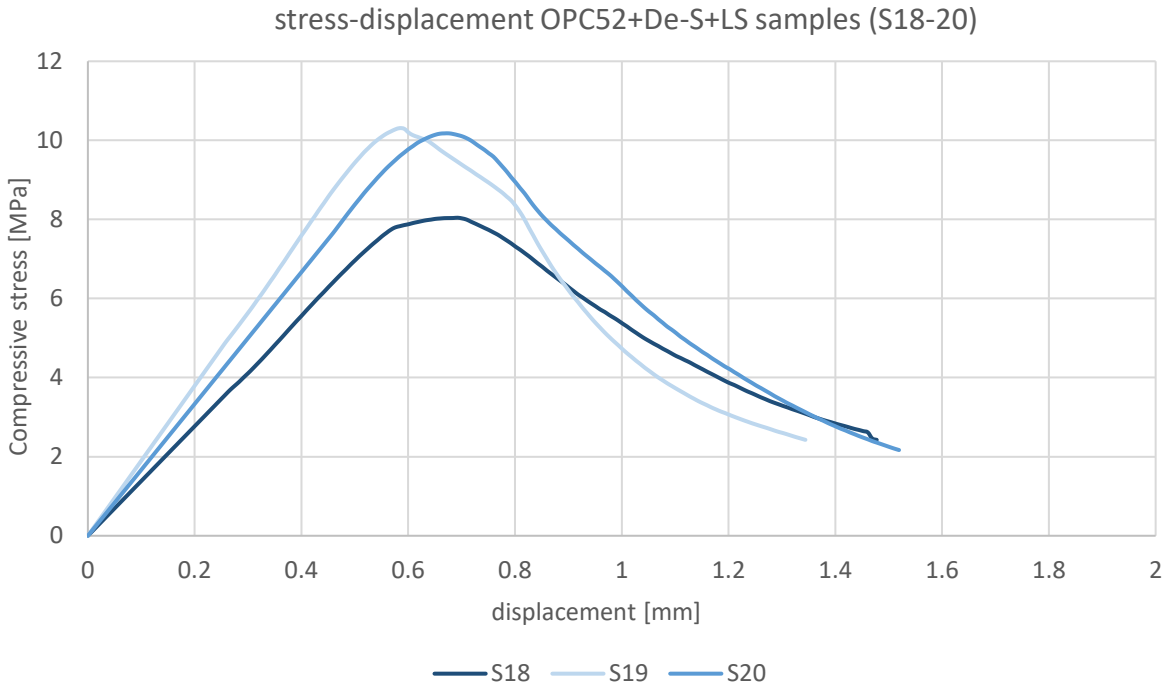

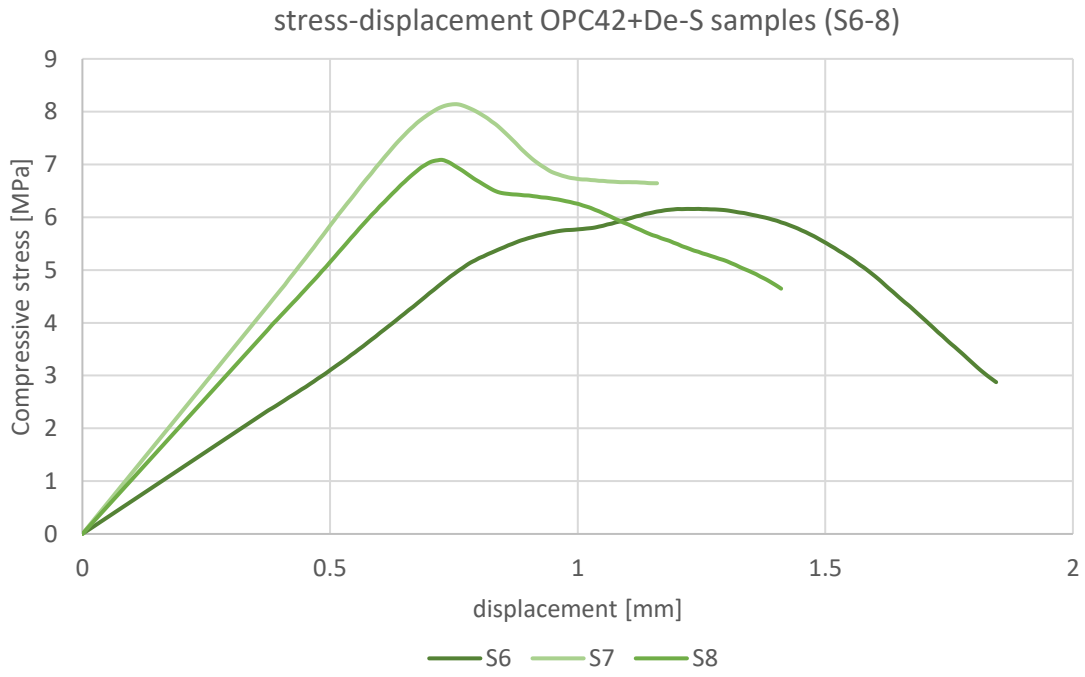

A.3 Samples post-aging (28 cycles)

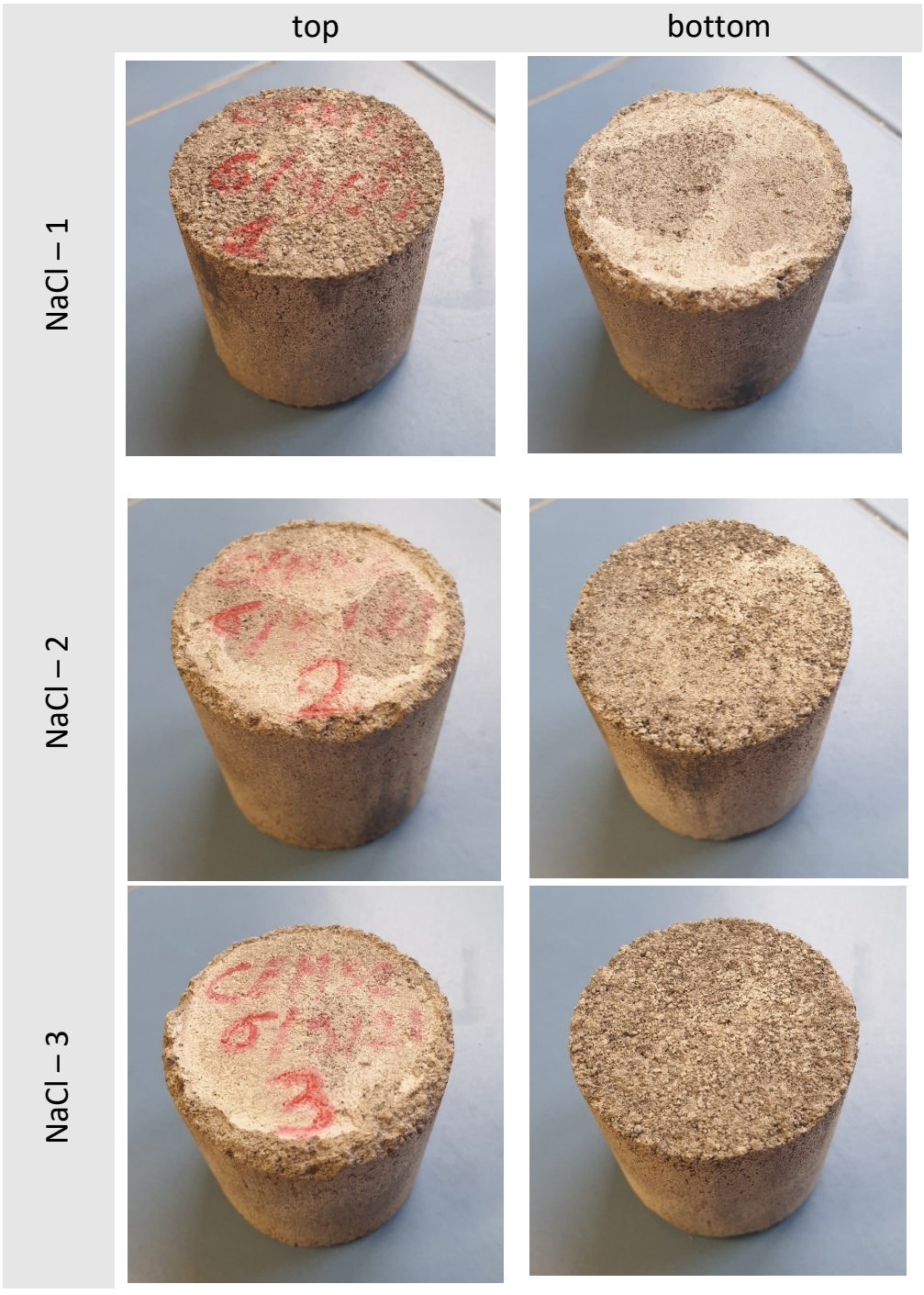

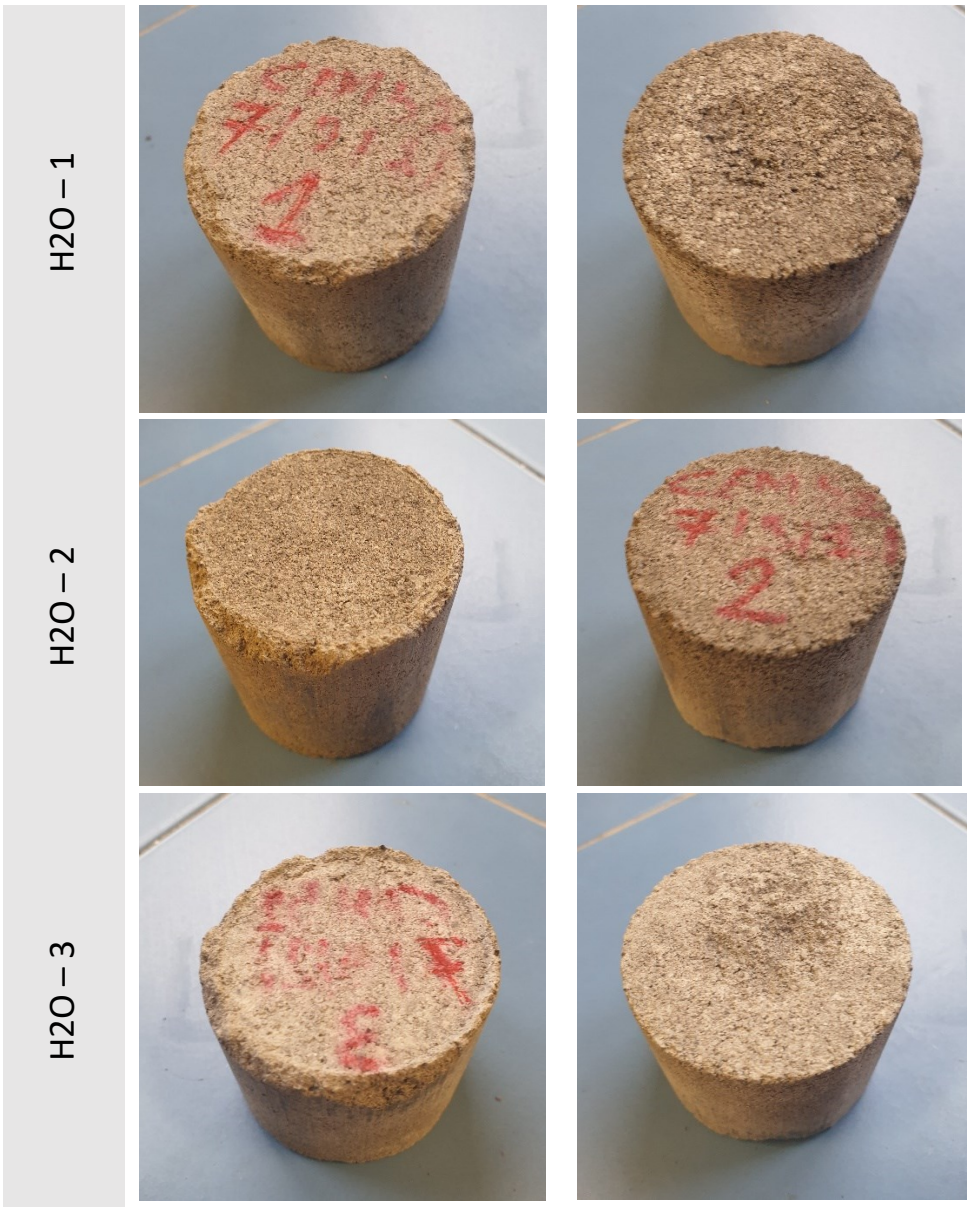
H2O – 1
H2O – 2
H2O – 3

12. Works Cited

12.1 Standards Cited

ASTM C42/C42M – 20
Standard Test Method for Obtaining and Testing Drilled Cores and Sawed Beams of Concrete.

ASTM C39/C39M - 21
Standard Test Method for Compressive Strength of Cylindrical Concrete Specimens

ASTM C666/C666M – 15
Standard Test Method for Resistance of Concrete to Rapid Freezing and Thawing

ACI 318-08
Building Code Requirements for Structural Concrete

BS 8007:1987
Code of practice for design of concrete structures for retaining aqueous liquids.

GB/T 50082
Standard for test methods of long-term performance and durability of ordinary concrete

EN 13877-2:2013
Concrete pavements. Functional requirements for concrete pavements

EN 15978:2011
Sustainability of construction works. Assessment of environmental performance of buildings.

EN 998-2:2016
Specification for mortar for masonry.

EN 1015-11:2019
Methods of test for mortar for masonry. Determination of flexural and compressive strength of hardened mortar

EN 206-1:2000
Concrete. Specification, performance, production and conformity

EN 1992-1-1:2004+A1:2014
Eurocode 2: Design of concrete structures. General rules and rules for buildings

EN 13877-1:2013
Concrete pavements. Materials

PD CEN/TS 12390-9:2016
Testing hardened concrete. Freeze-thaw resistance with de-icing salts. Scaling

12.2 Other References

Terrones-Saeta, J. M., Suárez-Macías, J., Iglesias-Godino, F. J. & Corpas-Iglesias, F. A., 2021. Evaluation of the Physical, Chemical and Environmental Properties of Ladle Furnace Slag for Their Utilization as Filler in Bituminous Mixtures. *metals,* 11(466).

Yildirim, I. Z. & Prezzi, M., 2011. Chemical, Mineralogical, and Morphological Properties of Steel Slag. *Advances in Civil Engineering.*

(CSI), T. C. S. I., 2016. *Getting the Numbers Right (GNR),* s.l.: wbcsd.

Anastasiou, E. K., Liapis, A. & Papachristoforou, M., 2017. Life Cycle Assessment of Concrete Products for Special Applications Containing EAF Slag. *Procedia Environmental Sciences,* Volume 38, pp. 469-476.

Andersson, R., Stripple, H., Gustafsson, T. & Ljungkrantz, C., 2019. Carbonation as a method to improve climate performance for cement based material. *Cement and Concrete Research.*

Arash, S., 2012. *MECHANICAL PROPERTIES OF MASONRY SAMPLES FOR THEORETICAL MODELING.* Florianópolis, 15th International Brick and Block Masonry Conference.

Bentz, D., Garboczi, E., Haecker, C. & Jensen, O., 1999. Effects of cement particle size distribution on performance properties of Portland cement-based materials. *Cement and Concrete Research,* Volume 29, pp. 1663-1671.

Bineshian, H., 2014. *Failure and post-failure aspects of mechanical response of concrete structures to compression and tension,* s.l.: The University of Western Austrialia.

Bogala, M. R., Zhang, M. & Reddy, R. G., 2015. *Characterization of Steelmaking Desulfurization Slag,* s.l.: Characterization of Minerals, Metals, and Materials.

Bogas, J. A., De Brito, J. & Ramos, D., 2016. Freeze–thaw resistance of concrete produced with fine recycled concrete aggregates. *Journal of Cleaner Production,* Volume 115.

Byun, S.-H.et al., 2010. Effect of Cement Particle Size on Properties of Ordinary Portland Cement. *Journal of the Korean Ceramic Society,* Volume 47.

Carpinteri, A. & Ingraffea, A., 1984. *Fracture mechanics of concrete: Material characterisation and testing.* The Hague: Martinus Njihoff Publishers.

Cembureau, 2015. *Building carbon neutrality in Europe,* s.l.: s.n.

Cembureau, 2018. *Thermal Energy Efficiency.* [Online]
Available at: https://lowcarboneconomy.cembureau.eu/5-parallel-routes/energy-

efficiency/thermal-energy-efficiency
[Accessed January 2021].

Chen, X., Huang, W. & Zhou, J., 2012. Effect of moisture content on compressive and split tensile strength of concrete. *Indian Journal of Engineering and Materials Sciences,* Volume 19.

Chen, Y., Davalos, J. F., Indrajit, R. & Kim, H.-Y., 2007. Accelerated aging tests for evaluations of durability performance of FRP reinforcing bars for concrete structures. *Composite Structures,* March.

Chen, Y.-L., Ko, M.-S., Chang, J.-E. & Lin, C.-T., 2018. Recycling of desulfurization slag for the production of autoclaved aerated concrete. *Construction and Building Materials,* Volume 158.

Consoli, N. C., Scheuermann Filho, H. C., Segadaes, L. & Cristelo, N., n.d. *Effect of wet-dry cycles on the durability, strength and stiffness of granite residual soil stabilised with Portland cement.* s.l., s.n.

CSI/ECRA, 2017. *Development of State of the Art Techniques in Cement Manufacturing: Trying to Look Ahead,* Düsselforf, Geneva: European Cement Research Academy.

European Commission, 2021. *2030 Climate and Energy Framework.* [Online]
Available at: https://ec.europa.eu/clima/policies/strategies/2030_en
[Accessed January 2021].

European Environment Agency, 2021. *Greenhouse gas emission intensity of electricity generation by country.* [Online]
Available at: https://www.eea.europa.eu/data-and-maps/daviz/co2-emission-intensity-9/#tab-googlechartid_googlechartid_googlechartid_chart_1111
[Accessed 27 10 2021].

European Environment Agency, 2021. *Greenhouse gas emission intensity of electricity generation by country,* s.l.: s.n.

Frigione, G. & Marra, S., 1976. Relationship between particle size distribution and compressive strength in portland cement. *Cement and Concrete Research,* Volume 6.

Gad, E. A. M., Habib, A. O. & Mousa, M. A., 2018. Understanding the mechanism of decomposition reactions of neat and superplasticized ordinary Portland cement pastes using thermal analysis. *Journal of Silicate Based and Composite Materials,* January.Volume 70.

Gyurkó, Z. & Nemes, R., 2020. Specimen size and shape effect on the compressive strength of normal strength concrete. *Periodica Polytechnica Civil Engineering,* 64(1).

Hossen, B., Islam, A. & Jadid, R., 2015. *Effect of specimen size on compressive strength of concrete.* Dhaka, First International Conference on Advances in Civil Infrastructure and Construction Materials.

Huijgen, W. J. J., Witkamp, G.-J. & Comans, R. N. J., 2005. Mineral CO2 Sequestration by Steel Slag Carbonation. *Environmental Science and Technology.*

Inventory of Carbon and Energy (ICE), 2019. *ICE Cement, Mortar and Concrete Model,* s.l.: s.n.

Juenger, M. C. G., Snellings, R. & Bernal, S. A., 2019. Supplementary cementitious materials: New sources, characterization, and performance insights. *Cement and Concrete Research.*

Levi, P., Vass, T., Mandova, H. & Gouy, A., June 2020. *Cement,* s.l.: International Energy Agency.

Librandi, P. et al., 2019. Mechanical and environmental properties of carbonated steel slag compacts as a function of mineralogy and CO2 uptake. *Journal of CO2 Utilisation.*

Lima, P. R., Toledo Filho, R. D. & Melo Filho, J. A., 2014. Compressive stress-strain behaviour of cement mortar-composites reinforced with short sisal fibre. *Materials Research,* 17(1).

Ma, F., Sha, A., Yang, P. & Huang, Y., 2016. The Greenhouse Gas Emission from Portland Cement Concrete Pavement Construction in China. *International Journal of Environmental Research and Public Health,* 13(7).

Mahoutian, M., Ghouleh, Z. & Shao, Y., 2014. Carbon dioxide activated ladle slag binder. *Construction and Building Materials.*

Mann, D. A., 2014. *The effects of utilising silica fume in portland cement pervious concrete,* Kansas City: University of Missouri.

Mendelson, M., 2018. *Effects Of Repeated Wet-Dry Cycles On Compressive Strength Of Fly-Ash Based Recycled Aggregate Geopolymer Concrete,* Florida: Florida Atlantic University.

MPA mortar, 2020. *Mortar Testing.* London: s.n.

Neville, A. M., 1996. *Properties of Concrete.* London: John Wiley and Sons, Inc..

Nguyen, H. et al., 2019. Byproduct-based ettringite binder - a synergy between ladle slag and gypsum. *Construction and Building Materials.*

Nguyen, H. et al., 2019. Ettringite-based binder from ladle slag and gypsum – The effect of citric acid on fresh and hardened state properties. *Cement and Concrete Research.*

Nguyen, H. et al., 2021. On the retardation mechanisms of citric acid in ettringite-based binders. *Cement and Concrete Research,* Volume 140.

OECD/IEA, CSI, 2018. *Low-carbon Transition in the Cement Industry: Technology Roadmap,* Paris: International Energy Agency.

Quaghebeur, M., Nielsen, P., Horckmans, L. & Van Mechelen, D., 2015. Accelerated Carbonation of Steel Slag Compacts: Developement of High-Strength Construction Materials. *Carbon Capture, Storage and Utilisation.*

Rangel, C. S. et al., 2020. Influence of Wetting and Drying Cycles on Physical and Mechanical Behavior of Recycled Aggregate Concrete. *materials.*

Research, Development and Technology Turner-Fairbank Highway Research Center, 2002. *Accelerated Aging of Concrete: A literature review,* s.l.: US Department of Transportation.

Richardson, J., 2016. *Soil Classification.* [Online]
Available at:
http://richardson.eng.ua.edu/Former_Courses/CE_340_su16/Notes/Soil_Classification.pdf
[Accessed 05 10 2021].

Schneider, M., 2019. The cement industry on the way to a low-carbon future. *Cement and Concrete Research.*

Scrivener, K., Vanderley, J. & Gartner, E., 2018. Eco-efficient cements: Potential economically viable solutions for a low-CO2 cement-based materials industry. *Cement and Concrete Research.*

Setzer, M., Fagerlund, G. & Janssen, D., 1996. CDF Test – Test method for the freeze-thaw resistance of concrete with sodium chloride solution (CDF). *Materials and Structures,* November.pp. 523-528.

Smarzewski, P., 2019. Processes of Cracking and Crushing in Hybrid Fibre Reinforced High-Performance Concrete Slabs. *processes,* 7(1).

Sudin, M. & Ramli, M., 2014. *Effect of Specimen Shape and Size on the Compressive Strength of Foamed Concrete,* s.l.: EPD Sciences.

Sugrañez, R. et al., 2013. Controlling microstructure in cement based mortars by adjusting the particle size distribution of the raw materials. *Construction and Building Materials,* Volume 41.

TA Instruments, 2011. *TGA Brochure Thermal Analysis.* [Online]
Available at: http://www.tainstruments.com/pdf/brochure/2011%20TGA%20Brochure.pdf
[Accessed 10 2021].

Tantawy, M. A., 2017. Effect of High Temperatures on the Microstructure of Cement Paste. *Journal of Materials Science and Chemical Engineering,* Volume 5.

Teo, P. T., Zakira, S. K., Salleh, S. Z. & et. al., 2020. Assessment of Electric Arc Furnace (EAF) Steel Slag. *Metals.*

The Concrete Society, 2014. Water absorption limits on aggregates.

Thomas, M., 2007. *Optimizing the Use of Fly Ash in Concrete,* Illinois: Portland Cement Association.

Tiwari, A., 2015. *How can I interpret a TGA graph?* [Interview] 2015.

Tokyay, M. & Özdemir, M., 1997. Specimen shape and size effect on the compressive strength of higher strength concrete. *Cement and Concrete Research,* 27(8).

Valenza II, J. J. & Scherer, G. W., 2007. A review of salt scaling: II. Mechanisms. *Cement and Concrete Research.*

Wang, D., Chang, J. & Ansari, W. S., 2019. The effects of carbonation and hydration on the mineralogy and microstructure of basic oxygen furnace slag products. *Journal of CO2 Utilisation.*

Wang, X. et al., 2019. Carbonation of steel slag and gypsum for building materials and associated reaction mechanisms. *Cement and Concrete Research.*

Yoon, J., Kim, J. H., Hwang, Y. Y. & Shin, D. K., 2015. Lightweight Concrete Produced Using a Two-Stage Casting Process. *Materials,* 8(4).

Zajac, M. et al., 2020. Phase assemblage and microstructure of cement paste subjected to enforced, wet carbonation. *Cement and Concrete Research.*

Zeng, X. H. et al., 2016. A study of the dynamic mechanical properties of CRTS I type CA mortar. *Construction and Building Materials,* 112(2).

Zhang, S., Dong, X., Zhang, H. & Deng, M., 2014. Research on Deterioration Mechanism of Concrete Materials in an Actual Structure. *Advances in Materials Science and Engineering.*